CONSISTENCY OF GLOBAL MODIS AEROSOL OPTICAL DEPTHS OVER OCEAN ON TERRA AND AQUA CERES SSF DATASETS

Alexander Ignatov[1], Patrick Minnis[2], Walter F. Miller[2,3], Bruce A. Wielicki[2], Lorraine Remer[4]

[1]*NOAA/NESDIS, Office of Research and Applications,*

E/RA3, Rm.603, WWB, 5200 Auth Rd., Camp Springs, MD 20746-4304, USA

[2]*NASA/LaRC, Atmospheric Sciences, Hampton, VA 23681, USA*

[3]*Science Applications International Corporation (SAIC), Hampton, VA 23666*

[4]*NASA/GSFC, Greenbelt, MD 20771, USA*

Corresponding author's address: Dr. Alex Ignatov
phone (301)763-8053 (x190)
fax (301)763-8052
email: *Alex.Ignatov@noaa.gov*

E/RA3, Rm.603, WWB
NOAA
5200 Auth Road
Camp Springs, MD 20746-4304

Submitted for publication, Section "Articles", Journal of Geophysical Research

03 September 2005 *Manuscript received*:

Abstract

Aerosol retrievals over ocean from the Moderate Resolution Imaging Spectroradiometer (MODIS) onboard *Terra* and *Aqua* platforms are available from the Clouds and the Earth's Radiant Energy System (CERES) Single Scanner Footprint (SSF) datasets generated at NASA Langley Research Center (LaRC). Two aerosol products are reported side-by-side. The *primary* M product is generated by sub-setting and re-mapping the multi-spectral (0.47-2.1 μm) MODIS produced oceanic aerosol (MOD04/MYD04 for *Terra/Aqua*) onto CERES footprints. M*D04 processing uses cloud screening and aerosol algorithms developed by the MODIS science team. The *secondary* AVHRR-like A product is generated in only two MODIS bands 1 and 6 (on *Aqua*, bands 1 and 7). The A processing uses the CERES cloud screening algorithm, and NOAA/NESDIS glint identification, and single-channel aerosol retrieval algorithms. The M and A products have been documented elsewhere and preliminarily compared using 2 weeks of global *Terra* CERES SSF Edition 1A data in which the M product was based on MOD04 collection 3. In this study, the comparisons between the M and A aerosol optical depths (AOD) in MODIS band 1 (0.64 μm), τ_{1M} and τ_{1A} are re-examined using 9 days of global CERES SSF *Terra* Edition 2A and *Aqua* Edition 1B data from 13 - 21 October 2002, and extended to include cross-platform comparisons. The M and A products on the new CERES SSF release are generated using the same aerosol algorithms as before, but with different preprocessing and sampling procedures, lending themselves to a simple sensitivity check to non-aerosol factors. Both τ_{1M} and τ_{1A} generally compare well across platforms. However, the M product shows some differences, which increase with ambient cloud amount and towards the solar side of the orbit. Three types of comparisons conducted in this study - cross-platform, cross-product, and cross-release – confirm the previously made observation that the major area for improvement in the current aerosol processing lies in a more formalized and standardized sampling (and most importantly, cloud screening) whereas optimization of the aerosol algorithm is deemed to be an important yet less critical element.

1. Introduction

To improve our understanding of the relationships between the Earth's radiation budget and clouds and aerosols, the *Terra* and *Aqua* satellites carry, in addition to other instruments, four Clouds and the Earth's Radiant Energy System (CERES) scanners to measure the radiant energy exchange on Earth [*Wielicki et al.* 1996]. CERES flight models 1 and 2 (FM1-2) have been operating on *Terra* since its launch into a 1030 Local Time (LT) Sun-synchronous orbit in December 1999. *Aqua*, launched into a 1330 LT orbit in May 2002, carries flight models 3 and 4 (FM3-4). The CERES Science Team generates Single Scanner Footprint (SSF) climate data records by combining CERES radiances with cloud and aerosol retrievals from the MODerate resolution Imaging Spectro-radiometers (MODIS) also onboard *Terra* and *Aqua* [*Geier et al.* 2003]. Mean and standard deviation of the finer resolution imager pixel radiances are calculated separately from the clear and cloudy portions of every CERES field-of-view (FOV) and reported in (larger size) CERES footprints, along with cloud/aerosol retrievals from these radiances. The spatial resolution (equivalent diameter at nadir) is 0.25-1 km for MODIS and ~20 km for CERES.

These SSFs constitute an extremely valuable product for addressing the relationships between radiation and aerosols, not only because the essential parameters are well-matched in time and space, but also because they are providing a relatively long and continuous time series of measurements taken at two different times of day. To ensure that these products can be used confidently for studies of climate-scale processes and diurnal changes, it is necessary to characterize the consistency of the retrieved parameters over time, across platforms, between processing releases, and between different algorithms. The consistency of the broadband radiance data and the CERES cloud retrievals have been described elsewhere [e.g., *Szewczyk et al.* 2005, *Minnis et al.* 2004]. *Ignatov et al.* [2005] performed a preliminary analysis of an early release of the aerosol products on the *Terra* SSFs, but since then new product releases and *Aqua* data have become available requiring a more in-depth characterization of the CERES aerosol products. This paper examines, in detail, the similarities and differences between the aerosol optical depths (AOD) derived from *Terra* and *Aqua* collection 4 MODIS data and convolved into the CERES SSFs.

Over ocean, two aerosol products are reported for each CERES footprint on the SSF, both derived from MODIS, yet using different sampling and aerosol algorithms [*Ignatov et al.* 2005]. The *primary* M product is derived from the standard M*D04 granules (termed MOD04 for *Terra* and MYD04 for *Aqua*), developed by the MODIS Science Team, whereas a simpler *secondary* AVHRR-like A product is produced by the CERES Science Team with a less sophisticated cloud clearing, more restrictive glint screening and a single-channel NESDIS aerosol algorithm. The A product serves as a backup for the M product. Also, it is helpful to place the 27+ year NOAA AVHRR, and the 7+ year Tropical Rainfall Measuring Mission (TRMM) Visible and Infra-Red Scanner (VIRS) heritage aerosol records in context of the more accurate M aerosols, and to quantify the MODIS multi-channel improvements. The M and A products on the *Terra* and *Aqua* CERES SSF datasets were described in detail by *Ignatov et al.* [2005] and are only briefly summarized in section 2 below.

This study cross-compares M and A AOD retrievals in MODIS band 1, τ_{1M} and τ_{1A}, respectively, from the two platforms using global CERES SSF *Terra* Edition 2A and *Aqua* Edition 1B data. The cross-product comparisons (M vs. A) performed by *Ignatov et al.* [2005] with the previous release *Terra* CERES SSF data, are reexamined here with the latest and improved SSF release, and the analyses are extended to include the newly available *Aqua* data. There was no change in either of the M or A aerosol algorithms (i.e. inversion of MODIS radiances to aerosol parameters). All changes between the two SSF releases were in the respective preprocessing (such as calibration or normalization of satellite radiances to solar flux) and sampling (i.e., selection of the *aerosol* pixels to be used in the aerosol inversions) procedures resulting in some differences in both aerosol products. This fact reiterates that sampling and preprocessing are critically important for the quality of AOD products [*Ignatov et al.* 2005].

2. Two aerosol products over ocean on the CERES SSF datasets

The *primary* M aerosol product is generated by sub-setting and remapping the 10-km M*D04 granules onto ~20-km (at nadir) CERES footprints. The M*D04 processing uses sophisticated cloud

screening and multispectral (6 bands from 0.55-2.1 μm) aerosol retrieval algorithms developed by the MODIS cloud and aerosol groups [*Ackerman et al.* 1998; *Tanré et al.* 1997; *Martins et al.* 2002; *Remer et al.* 2005]. Fifteen of the 29 aerosol parameters reported in each M*D04 granule over ocean are saved on the CERES SSF; only one of them is analyzed in this study, the M aerosol optical depth (AOD), τ_{1M}, reported at the central wavelength of MODIS band 1, λ_{1M}=0.644 μm.

The *secondary* A product uses a different glint and cloud screening and a simpler AVHRR-like 3rd generation NESDIS aerosol algorithm [*Ignatov et al.* 2005]. Two AODs, τ_{1A} (0.630 μm) and τ_{2A} (1.610 μm) are derived from MODIS bands 1 and 6 using two independent single-channel algorithms. (On *Aqua*, τ_{2A} at 2.113 μm is derived from band 7.) The respective look-up-tables were calculated separately for *Terra* and *Aqua*, taking into account the exact spectral response functions of their MODIS sensors. Only τ_{1A} is analyzed in this study reported at the wavelength λ_{1A}=0.630 μm.

The A aerosol algorithm is currently employed to analyze data from AVHRR/3 on the NOAA-16, -17 and -18 platforms, VIRS on TRMM, and MODIS on *Terra* and *Aqua* [*Ignatov et al.* 2004b; *Ignatov et al.* 2005]. More recently, it was tested using data from the Spinning Enhanced Visible and Infra-Red Imager (SEVIRI) onboard Meteosat Second Generation (MSG; renamed to Meteosat 8 after launch in 2002), the first successful test of the A algorithm with geostationary data [*Brindley and Ignatov* 2005]. Note that all A products, derived from different platforms and sensors (NOAA/AVHRR, TRMM/VIRS, *Terra* and *Aqua* MODIS, and MSG/SEVIRI), are consistently reported at standard wavelengths representative of the band centers for a generic AVHRR sensor, making different τ_A products fully comparable.

In both products, sun glint areas are excluded by only making retrievals outside the γ=40° cone glint angle. *Additionally*, all data from the solar side of the orbit are excluded in the A product for historical reasons. This restriction reduces the number of A samples compared to the M samples and is currently being re-evaluated.

The cross-platform comparisons include a 3-hr time difference between the mid-morning *Terra* and early afternoon *Aqua* platforms. Figure 1 shows that since their launch, *Terra* and *Aqua* have typically

been crossing the equator within 15 and 5 minutes of their nominal equatorial crossing times, respectively. However, local solar time of the aerosol observations may be shifted by an hour or two with respect to the equator crossing time due to the MODIS cross-track scan, the satellite orbital inclination, and product specifics (see example in Figure 2). According to *Kaufman et al.* [2000], AOD diurnal variations over open oceans are small, however, and should not affect results of cross-platform comparisons.

3. Data

This study uses 9 days of global *Terra* CERES/FM1 (Edition 2A) and *Aqua* CERES/FM4 (Edition 1B) SSF M and A aerosol data from 13-21 October 2002. The CERES FM1 and FM4 datasets were chosen because both instruments operated in a cross-track mode during October 2002, thereby providing uniform coverage, whereas their "twins", FM2 on *Terra* and FM3 on *Aqua*, operated in the rotating-azimuth-plane (RAP) mode. Aerosol products reported on the RAP SSFs on the same platforms are derived from the same MODIS instrument and therefore should be identical. But in fact, the fields of view of the two CERES instruments on the same satellite can significantly differ in size even though they are nearly collocated when scanning in the two modes. Geographical co-registration of the aerosol products reported at the centers of CERES footprints is more accurate when the instrument is in a cross-track mode and the CERES FOVs are generally smaller [*Ignatov et al.* 2005].

To evaluate aerosol improvements in this new SSF release (*Terra* Edition 2A and *Aqua* Edition 1B), we employ data for the same 9-day period, but from the previous SSF release (*Terra* Edition 1A and *Aqua* Beta1). The SSF Beta versions are not considered official by the CERES Science Team and not approved for public distribution. However, an exception to this rule was made here because no official *Aqua* SSF data are available based on the previous SSF processor, whereas the *Aqua* Beta1 processor was similar to that used for *Terra* Edition 1A.

The M and A SSF processing uses 1-km resolution MODIS L1b data as input and first sub-samples them in every N^{th} row and M^{th} pixel, to save disk space and processing time. The current SSF

processor subsets every 4th pixel in every 2nd line (N=2, M=4), whereas the previous processor saved every 2nd pixel in every 2nd line (N=2, M=2).

Then M aerosol properties are assigned to each sub-sampled MODIS pixel (from the 10-km M*D04 granule that contains that pixel) and the A "aerosol pixels" are identified by the A cloud and glint screening. One of the most important cloud tests in the A aerosol processing is the spatial uniformity test. It is applied to 2×2 arrays of *sub-sampled* pixels and requires that the difference between the maximum and minimum reflectances in MODIS band 1 does not exceed 0.003 (0.3%). As a result, the new test is more conservative because the same threshold is now applied to pixels separated by 4×8km compared to the previous separation of 4×4km. The M*D04-processing also employs a spatial uniformity test applied to 3×3 arrays of 1-km MODIS reflectances in band 4 (0.555 μm) with a requirement that the standard deviation is less than 0.0025 (0.25%) for the central pixel to be considered cloud-free. The thresholds used in these most critical cloud tests for aerosol retrievals over oceans are constants in both the A and M processing systems, i.e., they are assumed globally non-variable and independent of view and illumination geometry.

Next, the (sub-sampled) pixel-level M aerosol properties and the A screened radiances are convolved into the corresponding CERES footprint using the CERES point spread function, and the A aerosol properties are derived from the convolved radiances [*Geier et al.* 2003]. To reduce processing time and data volume, certain CERES footprints are removed in the new SSF release. A given CERES footprint may overlap the adjacent footprint by up to 80%, especially for the near-nadir footprints. Thus, thinning out highly overlapped CERES FOVs is expected to have a minimal impact on gridded products. The specifics of the sampling algorithm and its evolution can be found at http://eosweb.larc.nasa.gov/GUIDE/dataset_documents/cer_ssf_trmm_pfm_edition1.html.

There are other changes in the M and A products, in addition to the SSF sampling changes. The M processing in the previous *Terra* Edition 1A SSF release was based on an earlier MOD04 collection 3, whereas the *Aqua* Beta1 was based on MYD04 collection 4. The new SSF release consistently uses collection-4 products from both platforms (for a complete history of M*D04 product evolution, see

http://modis-atmos.gsfc.nasa.gov/MOD04_L2/history.html). The A product in the new SSF release uses reflectances calculated from radiances using more accurate solar constants (see section 5.3 for details). It is important to note however that there was no change in either M or A aerosol inversion algorithm from one SSF release to the other.

In this study, we concentrate on detailed analyses of the M and A retrievals in MODIS band 1 only, including evaluating the effect of new-release changes on τ_{1A} and τ_{1M}. Note that in the SSF datasets, the values of τ_{1M} and τ_{1A} are reported at slightly different wavelengths: λ_{1M}=0.644 and λ_{1A}=0.630 μm, respectively. For the present comparisons, τ_{1A} was first re-scaled to the M wavelength of 0.644 μm using the fixed A aerosol model as $\tau_{1A}(0.644\ \mu m) = 0.96377 \times \tau_{1A}(0.630\ \mu m)$ so that all τ_1's in this report are given at the reference monochromatic wavelength of λ_{1M}=0.644 μm [*Ignatov et al.* 2005].

Besides τ_{1M}, the M product reports six additional AODs in the MODIS aerosol bands 2-7 and the A product reports a second AOD, τ_{2A} [*Ignatov et al.* 2005]. However, these additional AOD data are not analyzed here. The analyses are deliberately restricted to only one parameter in both products, τ_1 to keep this study in-depth yet simple and succinct. For instance, omitting τ_{2A}'s [which are retrieved from different MODIS bands on *Terra* (6) and *Aqua* (7)] eliminates the need to re-scale them for cross-platform comparisons.

The inoperative *Aqua*/MODIS band 6 is excluded not only from the A processing but from the MYD04 processing, too. Thanks to the flexibility of the M retrieval lookup tables, only a subset of bands can be used for retrievals (*Tanré et al.* 1997). Note however that MYD04 continues to report all seven AODs in MODIS bands 1-7, consistently with MOD04, the AOD in *Aqua*/MODIS band 6 being a mere interpolation to λ=1.61 μm from the remaining 5 bands. [This treatment of band 6 on *Aqua* is fully analogous to band 3 (0.47 μm) on both platforms, which is not used in aerosol retrievals due to its high and variable surface reflectance, but AOD in this band is still reported on M*D04.] In evaluating the results of cross-platform τ_{1M}-comparisons below, one should keep in mind that the M aerosol algorithm, although identical for *Terra* and *Aqua*, is nevertheless applied to a different set of MODIS bands (6 on *Terra* and only 5 on *Aqua*). Off-line tests to quantify the effect of excluding band 6 (or any other band) on the τ_{1M}-

retrievals are possible using e.g. *Terra* MODIS data, where all six bands work nominally, but these analyses are beyond the scope of this study.

4. Summary global statistics

4.1 Statistics derived from CERES Field-of-Views (FOV)

The odd data rows in Table 1 list the global CERES FOV-based statistics of τ_{1M} and τ_{1A} from *Terra* and *Aqua*, along with associated local time, cloud amount, and retrieval geometry. Particular attention should be paid to the accurate definition of the cloud amount parameter, A_T, which was determined by the CERES Team cloud mask processing and is used throughout this paper. Its global statistics are listed in Table 1. Its M A_T counterpart is also available on the SSF but is not used here. For a given CERES footprint, the A cloud amount is defined as 100% minus percent fraction of those MODIS pixels within a FOV that were determined as "clear" by the CERES Team cloud mask processing. This definition may not be fully accurate, as not all "non-clear" pixels are necessarily "cloudy". Some of them may be simply missing (e.g. due to the scan edge) or poor quality data. These pixels are not included in the calculation. In addition, as pointed out by *Brennan et al.* [2005], the definition of "cloud amount" depends upon application. For instance, the fraction of clear pixels used in aerosol retrievals tends to be larger than one minus the fraction of cloudy pixels used in cloud retrievals, because either retrieval tends to classify questionable pixels in a counterpart category. Despite this tendency to be on a "safe side", *Brennan et al.* [2005] suggest that some fraction of the aerosol retrievals remains "cloud-contaminated" as well as some fraction of cloud retrievals is still "aerosol-contaminated".

For a particular FOV containing both M and A aerosol products, the A cloud amounts are identical. Their global statistics, shown in Table 1, differ, however, because many CERES FOVs have valid M retrievals but no A retrievals, and some FOVs have valid A aerosols with no corresponding M values. As a result, the global A_T statistics differ for the M and A products. Another specific feature of the A_T statistics used in this paper is that they are *conditional* and, therefore, biased estimates, since all

CERES FOVs with no clear pixels (i.e., A_T=100%) are ignored in calculations.

The following observations emerge from the CERES FOV statistics in Table 1:

(a) Cross-product sampling differences. The M sample size is twice that for the A product. This result is consistent with *Ignatov et al.* [2005]. Additional analyses (not shown) suggest that ~70% of this difference is due to excluding the solar side of the orbit and viewing zenith angles θ_V>60° in the A product, whereas the remaining ~30% is due to M/A cloud screening differences. Note that data in A_T-column of Table 1 show that the average fraction of cloudy pixels is ~15% larger in the M product than in the A product, which is consistent with the reduced A sample and indicates that cloud screening is more conservative in the A product than in the M product.

(b) Cross-platform sampling differences. The *Terra* results yield 11% more CERES FOVs with valid M-data than *Aqua*, and 2% fewer FOVs with valid A-data. (In cross-platform sample size comparisons one should keep in mind that out of the total of 216 hours, 3 hours of *Aqua* Edition 1B SSF data were missing (a 1.4% reduction) during this 9-day period because of CERES diagnostics.) The nature of the M cross-platform sampling differences is not immediately clear. Indeed, despite some orbital differences, *Terra* and *Aqua* cover almost identical geographical domains (Figures 4 and 5). Their cross-platform cloud amount differences are also small and consistent: $\Delta A_T = A_T(Terra) - A_T(Aqua)$ = 3.0% and 2.4% in the M and A products, respectively.

(c) Cross-product τ_1 differences. Generally, τ_{1A} is larger than τ_{1M}: τ_{1A}-τ_{1M}= 0.004 for *Terra* and 0.010 for *Aqua*. Presumably, the algorithm-induced positive bias in the A product would be even greater, if the data selection were not constrained by the more conservative A cloud-screening process [see analyses in section 6.1 below]. Data in Table 1 show the net effect of these two counterbalancing mechanisms.

(d) Cross-platform τ_1 differences. In both products, the mean AODs are greater from *Terra* than from *Aqua* data: $\Delta\tau_{1M}$ = 0.009 and $\Delta\tau_{1A}$ = 0.003. This bias could be real indicating a systematic decrease in marine aerosol concentrations from morning to afternoon. Or, it may be due to differences in the illumination geometry that are not properly modeled by the respective retrieval algorithm. The

mean value of θ_s for *Aqua*, is 5° less than that for *Terra*, and the respective scattering and glint angles are 3-4° larger than for *Terra*. The bias may also be due to residual cross-platform cloud screening differences (the *Aqua* screening is ~2-3% more conservative than *Terra*) or to a combination of viewing and screening differences.

4.2 Aggregating CERES FOV into gridded 1° product

For the analyses below, the global τ_1-retrievals and auxiliary parameters from 13 - 21 October 2002, reported for the CERES FOVs, were first remapped onto a regular grid and averaged, resulting in N = 164,895 and N = 81,426 1°-square boxes from *Terra*, and 145,395 and 80,573 from *Aqua*, with M and A aerosols, respectively. The 1°-average cloud amount A_T parameter was calculated using only those CERES FOVs with valid aerosol retrieval in them, ignoring footprints with A_T=100%. Figure 3 (top) shows histograms of CERES FOVs counts, N, used for calculating the average 1° statistics. The grid boxes are populated non-uniformly and the shapes of the histograms differ for the two products, due to differences in their sampling. Smaller values of N in a box are generally associated with more cloud or glint, or proximity to the coast line, scan edge, or sun illumination limits. Figure 3 (bottom) plots the respective τ_1(N)-trends in the retrievals. The most prominent features in Figure 3 are:

(a) Both τ_{1M}(N) and τ_{1A}(N) increase towards low N. Greater uncertainties are expected in a product when approaching the boundaries of its valid domain. Figure 3 suggests that such difficulties are better mitigated in the A product, which has flatter τ_{1A}(N) trends and more consistent across platforms.

(b) The minimum values of τ_{1A} are informative about performance of the A algorithm and the calibration of band 1. For instance, close agreement between the values of min(τ_{1A}) from *Terra* and *Aqua* indicates excellent calibration consistency between the two MODIS instruments. Simple estimates show that their bands 1 are consistent to within ~1-2% [*Ignatov* 2002]. Another interesting feature of Figure3 is the negative bias in min(τ_{1A}) towards small values of N. The A

algorithm does not truncate negative values of τ_{1A} (which may result from e.g. radiometric errors, or occur when *in situ* Rayleigh optical depth is smaller than assumed in the retrievals). The latter happens when the water surface is elevated above the sea level. For example, the smallest τ_{1A} are often associated with the least populated 1°-boxes, typically found over high-altitude lakes [*Ignatov and Stowe* 2002a]. In the M product, negative values of τ_{1M} are currently truncated and therefore provide no information [*Ignatov et al.* 2005].

(c) The $\tau_{1M}(N)$ trends in *Terra* and *Aqua* diverge for N<20 (where most M-data are found), possibly indicating residual cross-platform cloud screening differences. Exclusion of band 6 from *Aqua* processing, or possible calibration differences in the MODIS bands used in aerosol retrievals, either directly (bands 1-2 and 4-7) or indirectly (e.g. thermal IR bands used in cloud clearing), may also contribute to the observed differences. However, the contribution of each individual band (e.g. band 6) to the τ_{1M} product derived using the multi-spectral M algorithm, is unknown.

Global average statistics of τ_1 and auxiliary parameters based on the $(1°)^2$-data are listed in the even rows of Table 1. They differ systematically from their finer-resolution CERES FOVs counterparts. For instance, the global mean τ_1's derived from daily 1° data are all systematically higher than their CERES FOV-based counterparts. In the remaining part of this study, we concentrate on the analyses of 1° data, assuming that the effect of spatial scale does not alter the results of the comparisons, as long as consistent sampling and statistic (arithmetic or geometric) is used. The scale-dependence of the mean global AOD values calls for better understanding and proper handling of this effect on the aerosol signals.

5. Global maps and histograms of retrievals

5.1 Geographical distribution

Figure 4 shows global distributions of τ_{1M} and τ_{1A} from *Terra* or *Aqua* derived from 1° data averaged over the 9-day period. Despite large differences in the M and A sampling and aerosol algorithms and in the *Terra* and *Aqua* orbital configurations, all four products show remarkable agreement. Visually,

the largest differences are between the M-products from *Terra* and *Aqua* (note in particular the "roaring forties" of the Southern hemisphere). The A-products, on the other hand, are more consistent across platforms in area coverage, mean values of τ_{1A}, and spatial patterns. In general, the M and A products are similar, but agree better for *Aqua* than for *Terra*.

All four products are "blurred" around the costal lines, due to the large size of the CERES footprints. *Ignatov et al.* [2005] have shown that blurriness is even worse for CERES instruments in a rotated azimuth mode. Differences in the application of water-surface classification maps are apparent in the M and A products. The A product tends to have more data points over inland water bodies, such as the Caspian Sea and Lakes Baikal and Victoria, than the M product. The M*D04 processing does not calculate ocean aerosol in the $(10\ km)^2$ grid if even one pixel is over a land surface, whereas, the A product calculations only require the 1-km pixel being processed corresponds to a water surface. The respective τ_{1A} values, although present here, are however often unrealistic, being biased either high or low due to violations of the assumptions of the retrieval algorithm [*Ignatov and Stowe* 2002a]. An example of high τ_{1A}-bias is found over the Caspian Sea. Although a relatively large value of AOD is expected there, because it is a highly polluted basin, the Caspian Sea water is very turbid causing a bright surface reflectance that is interpreted as an elevated AOD. Collection 4 of the M*D04 product stopped reporting aerosol retrievals over much of the Caspian Sea after adding the turbidity test [*Remer et al.* 2005]. Examples of low τ_{1A}-bias are found e.g. over the two high-altitude lakes in China: the Namu (30°N, 90°E, h~4,700m) and the Koko Nor (37°N, 100°E, h~3,200m). The *in situ* Rayleigh optical depth at those altitudes is much smaller than used in the retrieval look-up-tables, which were created assuming that the water boundary is located at sea level. As a result, too much contribution is subtracted from the satellite radiance, driving the retrieved τ_{1A} below zero with values ranging from -0.07 to -0.05. *Ignatov and Stowe* [2002a] discuss in more detail the τ_{1A}-anomalies over bright and high-altitude inland waters.

Figure 5 shows zonal sampling densities and variations in the AOD retrievals. Cross-platform differences are smaller and more spatially localized in the A product. Both products yield low values at high latitudes. These areas are generally clean and have low AOD, but they are also associated with low

solar elevations and may be biased due to the increased complexity of cloud screening and possible violations of the plane-parallel assumption in the 6S radiative transfer model that was used to generate the look-up-tables [*Ignatov and Stowe* 2002a]. In the CERES SSF data, both the M and A retrievals are reported if $\theta_S < 70°$. Assessment of the θ_S bias, if any, caused by modeling inadequacies, would require sampling the same areas over the full range of the daily θ_S cycle. This is best achieved from geostationary platforms, e.g. [Brindley and Ignatov 2005]. For satellites in near-polar orbits, the latitude and θ_S are correlated, so it is not possible to evaluate the possible θ_S dependency using *Aqua* and *Terra*. Data from a satellite, such as *TRMM*, with a precessing orbit are needed to examine the solar-zenith-angle effect. This topic will be addressed in a future study using the *TRMM* VIRS data.

5.2 Histograms of τ_1

Plots τ_1 of probability density functions (PDF) derived from the 1°-data are shown at the top of Figure 6. Their shapes are close to the lognormal distribution [*O'Neill et al.* 2000, *Ignatov and Stowe* 2002, *Matthias and Bösenberg* 2002]. *Geometric* τ-statistics are also superimposed. They systematically differ from their *arithmetic* counterparts listed in Table 1, due to τ-lognormality. However, if a consistent statistic (arithmetic or geometric) is considered, then the mean values of τ_1 are typically within ~±0.01 of each other from either M or A product and *Terra* or *Aqua* platform. According to Table 1 and Figure 6, the global mean cross-platform differences in τ_{1A} are a factor of ~3-7 smaller than in τ_{1M}. This result agrees with the qualitative observation from Figure 4 that the A product is more cross-platform consistent.

The frequency distributions are re-plotted in $\log(\tau_1)$ space at the bottom of Figure 6, which also shows their skewness (s) and kurtosis (k). Skewness characterizes the asymmetry of a distribution, while kurtosis provides a measure of the width relative to a normal distribution. All four PDFs show a negative skewness, $s < 0$ (i.e., left tails are heavier than the right tails), and a positive kurtosis, $k>0$ (i.e., they are peaked more than a Gaussian distribution). Overall, the τ_{1M}-PDFs are closer to a lognormal shape than the τ_{1A}-PDFs: the M skewness and kurtosis are factors of 3 and 10, respectively, smaller than in their A-counterparts.

5.3 Histograms of τ_1 from the previous SSF release

Figure 7 re-plots Figure 6 but using data from the previous SSF release. Although the *Aqua* M product is based on the same collection 4 MYD04 input, the M products on the two different SSF releases differ slightly. For instance, the global geometric mean τ_{1M} increased from 0.095 in the previous release to 0.102. This 7% rise in the global average AOD is simply due to a changed mapping of the same 10-km MYD04 product into the CERES footprints. Additionally, the new *Aqua* τ_{1M} deviates from a Gaussian shape more than the previous one, as manifested by the increased skewness and kurtosis. This example clearly shows the importance of using an objective and consistent sampling to ensure the quality of a given aerosol product, especially when it is part of a climate data records.

On the other hand, the *Terra* M product in the earlier release was based on MOD04 collection 3 data, whereas in Figure 6 it was based on collection 4. Clearly, cross-platform consistency has significantly improved when a consistent M*D04 collection 4 is used. We emphasize that here, this improvement is determined with simple cross-consistency checks without resorting to complex and time-consuming validation against ground based sun-photometers.

The improvement in the A product is more incremental than in the M product, but is statistically significant. The new A products agree better across platforms, and their histograms are narrower and closer to a lognormal shape. The difference between the A products shown in Figures 6 and 7 stems from two different factors. The first is the different sampling (4^{th} pixel/2^{nd} row in Figure 6 versus 2^{nd} pixel/2^{nd} row in Figure 7), which also affects the retrievals through a more stringent spatial uniformity test in the new release. Second, values of the solar constant used in the A processing have been corrected. In the previous release, the *TRMM*/VIRS solar constant, $F_o = 531.7$ $Wm^{-2}sr^{-1}\mu m^{-1}$, was mistakenly used to convert L1b radiances to reflectances for both *Terra* and *Aqua*. In the new release, this error was corrected and the following values are now used: $F_o = 511.3$ and 511.9 $Wm^{-2}sr^{-1}\mu m^{-1}$ for *Terra* and *Aqua*, respectively. This 4% reduction in the solar constants, equivalent to a calibration change, effectively raised the *Terra* and *Aqua* reflectances in the new release by 4% ($\varepsilon_1 \sim +0.04$) from the previous release. According to Ignatov

[2002], the effect of a calibration change on the retrieved AOD at 0.63 μm is estimated as $\Delta\tau_{1A}\sim(0.37+0.71\tau_{1A})\varepsilon_1$. For typical AOD over ocean with modal value of $\tau_{1A}\sim0.1$, and error $\varepsilon_1\sim+0.04$, the expected average increase in τ_{1A} is $\Delta\tau_{1A}\sim+0.02$. Note however that the new τ_{1A}-modal values in Figure 6 are only ~+0.01 larger than the old numbers in Figure 7. This is because about half of the expected calibration-induced τ_{1A}-change of $\Delta\tau_{1A}\sim+0.02$ was effectively offset by a more stringent cloud screening (i.e., the spatial uniformity test) in the new SSF release. The effect of cloud screening on AOD is further discussed in section 6.1 below.

6. Cloud amount and angular dependencies of retrievals

The data in Table 1 show that some auxiliary parameters, cloud amounts and viewing and illumination angles, associated with the retrievals systematically differ between the products and platforms. These differences may affect the products, if the retrieval algorithm performs non-uniformly over the full range of cloud conditions and retrieval geometry. In this section, these cross-platform and cross-product differences in the retrieval domains and their effect on aerosol retrievals are analyzed. Since the relationships between a given auxiliary parameter and AOD are estimated using only one week of data, they may be distorted by possibly misleading false correlations between different factors, which are not fully independent (for instance, low τ_{1M} and τ_{1A} at high sun $\theta_S>50°$ may come from clean high latitudes). Until a more representative dataset is used for analyses of such dependencies, we concentrate here on the comparison of domains in which retrievals are available in the two products and from the two platforms. The second focus is on the *cross-platform* consistency in the dependence of AOD on a given parameter when misleading correlations (if present) are expected to be minimized. Note that similar comparisons between the M and A products should also be deferred until the large differences in their respective samplings are resolved.

6.1 Cloud-Aerosol correlations

Figure 8 plots histograms of A_T and the variations of τ_1 with A_T. Figure 8 includes data only from those 1° boxes having at least one valid aerosol retrieval. In the A product, the relative proportion of such "aerosol-burden" grid boxes decreases with A_T as intuitively expected, whereas the increasing trend in the M product is counterintuitive. These different features in the M and A products, previously observed by *Ignatov et al.* [2005] and reproduced *Brennan et al.* [2005], may be due to artifacts in either the M or A cloud screening. Some regions with large A_T's may actually be extended areas (> 1°) with elevated AODs, which are misidentified as clouds by the more conservative A processing, but correctly identified as aerosols by the M processing. (For instance, the A panels in Figure 4 show more missing data in the center of the Saharan dust outbreak than the M panels.) Or, boxes with large A_T may be real cloud, which are correctly identified in the A processing but misidentified as aerosol by the less conservative M processing. (Such a scenario may explain the differences in the "roaring forties" in the Southern hemisphere, where the A cloud screening apparently does a better job than the M cloud screening.)

Sensitivity of τ_1 to the ambient cloud amount is significant in all four products. Similar cloud-aerosol correlations have been previously observed in the AVHRR, VIRS and, most recently, *Terra*/MODIS data [*Ignatov et al.* 2005]. Generally, $\tau_1(A_T)$ compares better across platforms for the same product than across products from the same platform. The slope of $\tau_1(A_T)$ is a factor of ~2 smaller in the τ_{1A} than in τ_{1M}. This variation is consistent with the data in Table 1, which show that cross-platform A_T-differences are much smaller than the cross-product differences. At least part of the $\tau_1(A_T)$ variations may be due to real cloud-aerosol interactions. However the facts that their shape and magnitude are product-specific and that $\tau_{1M}(A_T)$ diverges between *Terra* and *Aqua* at large A_Ts, indicate an effect of residual cloud cover (cf. also the diverging trend in the $\tau_{1M}(N)$ at low N in Figure 3). Some actual morning-afternoon differences between the τs and cloud amounts from the two platforms may exist, due to the 3-hour time discrepancy. However, the $\tau_1(A_T)$ relationship is expected to hold from platform to platform, at least for the same product, irrespective of the physical mechanism(s) underlying this relationship. Recall that many of the current cloud screening procedures (including those used in the M and A aerosol production) are threshold-based, and have difficulty resolving sub-pixel clouds, a problem that is deemed

to be a continuous rather than a discrete process.

Figure 9 re-plots Figure 8 but using data from the previous SSF release. Clearly, the cross-platform consistency between the *Terra* M product has improved in the new release, which manifests itself in both more consistent A_T-histograms and $\tau_{1M}(A_T)$ variations. The changes in the A product are twofold. First, as a result of a more stringent spatial uniformity test, the drop-off in the A_T histograms starts at ~60% in the new release compared with ~75% in the previous release. Apparently, this change has reduced the proportion of CERES FOVs with high cloud amounts but it has not affected the $\tau_{1A}(A_T)$ behavior. The other difference is that the new τ_{1A} has increased by ~0.02 at A_T near 0%, due to eliminating the error in the solar constants.

6.2 Dependence on viewing and illumination geometry

Figures 10-13 show histograms (top panels) of viewing zenith (VZA; θ_V), solar zenith (SZA; θ_S), scattering (χ), and glint (γ) angles and AODs (bottom panels) as functions of the same angles. Note that viewing zenith angle is defined as negative on the solar side of the orbit and positive on the anti-solar side.

The retrievals are made in different angle domains in the two products and from the two platforms. Neither algorithm retrieves AOD within 40° of the glint angle around the specular point resulting in dips in their respective θ_V-histograms around nadir and truncation of the high sun angles in the θ_S-histograms (Figure 10). In addition, the A algorithm historically is not applied when $\theta_{VA} > 60°$ and on the solar side of the orbit ($\theta_{VA} \leq 0°$), whereas the M technique allows τ_M retrievals up to the scan edge on both sides of the orbit ($-66° \leq \theta_{VM} \leq 66°$). *Aqua* makes its retrievals at slightly larger SZAs (Figure 11), and, in the M product, over a smaller range of SZAs. This difference ranges of SZA's between the algorithms arises from the VZA limitations seen in Figure 10. Clearly, the large differences in the SZA domains for the two products significantly exceed cross-platform differences. Thus, more consistency should be sought between the M and A sampling algorithms.

Variations of AOD compare generally well cross-platform in both products, but develop cross-platform biases in certain domains of retrieval geometry. In particular, $\tau_{1M}(\theta_V)$ diverges on the solar side of

the orbit by ~0.03, whereas $\tau_{1A}(\theta_V)$ shows a ~0.02 anomaly in the vicinity of θ_V~20° (Figure 10). The $\tau_{1M}(\theta_S)$ variations are coherent, but biased by ~0.01 over the full range of SZA, whereas $\tau_{1A}(\theta_S)$ behaves similarly for both platforms except under a very high Sun ($\theta_S < 35°$). Both products decline at large SZAs ($\theta_S > 50°$), which, as noted earlier, may be due to a generally lower aerosol loading in the remote Southern hemisphere and, to increased retrieval errors at low Sun elevations.

The scattering angle $\tau_1(\chi)$ variations (Figure 12) are largely consistent in both products, whereas the glint angle behavior of $\tau_{1A}(\gamma)$ shows some cross-platform biases at high glint angles $\gamma > 95$-100°. In addition, the τ_{1M} means differ by as much as 0.02 when $\gamma < 65°$.

Overall, the analyses in this section reveal the effects of large sampling differences in the two products. Cross-platform inconsistencies are generally larger in the M product. Note that these results are based on a limited time domain. To cover a larger range of SZAs and scattering angles and to ensure that these results are representative, a dataset covering other months should be analyzed in the future.

7. Refined space-time match-up in the product comparisons

At least part of the cross-platform and cross-product τ_1-differences are due to the sampling differences since no attempt was made to precisely match the τ_1-data in space and time. For the analyses in this section, the 1° data from *Terra* and *Aqua* for both products have been merged by latitude, longitude, and day to form the respective match-up datasets. The respective four match-up datasets are defined as those containing the following [1°-1 day] boxes in which (a) the M product is available from both satellites (M *Terra/Aqua* intersection); (b) the A product is available from both satellites (A *Terra/Aqua* intersection); (c) both M and A products are available from *Terra* (*Terra* A/M intersection); (d) both M and A products are available from *Aqua* (*Aqua* A/M intersection). Two comments should be made before we proceed with the analyses of the match-up datasets below.

The time difference between *Terra* and *Aqua* remains and may affect results of cross-platform comparisons using the *Terra/Aqua* match-up datasets (both M and A) in section 7.1. Additionally, spatial

noise is also present in all four match-up files, as the 1° τ_1-averages actually come from different parts of the 1°-box and may be separated by up to 150 km. It affects the comparison statistics in sections 7.1 and 7.2. No attempt was made to quantify the effect of spatial and temporal noise on the results of comparisons. Instead, the focus is on the *relative*, rather than *absolute*, comparison statistics (correlation coefficient, R; bias, δ; and noise, σ), which are *equally* affected by the spatio-temporal mismatch errors.

The match-up datasets are *sub-samples* of the full dataset. For its statistics to hold over the full sample, the match-up must be representative of the full sample. A simple check of representativeness is required but often overlooked. For instance, validation statistics obtained from comparison with a limited number of sun-photometers, mostly in the coastal tropical areas, is assumed to represent the performance of the global satellite product, but this assumption is never checked [e.g., *Ignatov et al.* 1995; *Remer et al.* 2002, 2005; *Myhre et al.* 2004]. This question is further discussed in section 7.3.

7.1 Terra versus Aqua comparison

Cross-platform comparisons are useful to determine if the AOD is captured consistently from the two platforms. Table 2 shows that the M product is available from both *Terra* and *Aqua* in 96,275 [1 day-1°] boxes, whereas the A product is available from both platforms in only 29,742 boxes. These two *sub-samples* of the full M and A products are termed the "M *Terra/Aqua* intersection" and the "A *Terra/Aqua* intersection", respectively.

The top two panels of Figure 14 plot 'τ_{TERRA} vs. τ_{AQUA}' scattergrams from these two intersections. Cross-platform noise appears to be larger in the M product. The respective correlation coefficients are also superimposed: R=0.73 in the M and 0.80 in the A product.

Data points in the 'τ vs. τ' scattergrams are very non-uniformly distributed: the vast majority of points are found in the first quadrant close to the origin. Taking into account τ-lognormality, Figs. 14a2 and b2 re-plot the 'τ-τ' scattergrams as 'lgτ-lgτ'. The clusters are better constrained in a log-space. (Note that the A log-sample is reduced, because logarithm cannot be taken of 157 non-positive τ_{1A}, in either dataset, whereas the M log-sample remains unchanged because all $\tau_{1M} > 0$.) Interestingly, the log-

transformation improves correlation in the M product from R=0.73 to 0.76, but not in the A product, where the correlation actually drops from R=0.80 to 0.78. Nevertheless, the cross-platform correlation is larger in the log-scale A product, too.

The remaining panels in Figure 14 plot histograms of the *Terra-Aqua* τ-differences (a3 - b3), and lgτ-differences (a4 - b4). The A product shows a smaller cross-platform bias ($\delta = 0.003$ vs. 0.011) and noise ($\sigma = 0.048$ vs. 0.066) compared to the M product, and continues to be more cross-platform consistent, in both linear and log metrics. Note that the *contrast* between the smaller cross-platform noise in the A product relative to the greater noise in the M product can be improved if the spatio-temporal noise is removed from the data. Assuming for the sake of argument that the spatio-temporal noise, $\sigma_{ST} = 0.040$, is the same in both products, and that it is random and independent of other errors (so that the errors add up in a RMS sense), then the "true" cross-platform RMSDs are $\sigma_o = 0.026$ for the A product versus $\sigma_o = 0.052$ in the M product. Assuming that noise is equal from *Terra* and *Aqua*, the "true noise" in the τ_{1M} and τ_{1M} products can be estimated in a similar fashion as $\sigma_{oA} = 0.018$ and $\sigma_{oM} = 0.037$. These estimates are given here for illustration only. They will be defined more precisely when the σ_{ST} parameter is known.

7.2 M versus A comparison

Table 3 shows that there are 79,209 data points in which both products are available from *Terra*, and 77,262 such data points from *Aqua*. Figure 15 plots the results of cross-product comparisons similar to the cross-platform analyses in Figure 14. The M-A correlation is R~0.86-0.87, an improvement from *Terra* Edition 1A data where it was R~0.84 and 0.78 in December 2000 and June 2001, respectively. Cross-product scattergrams are more constrained in log-space, although the correlation is somewhat reduced. The two products show a systematic bias of $\delta \equiv (\tau_{1A} - \tau_{1M}) = 0.012 \pm 0.001$ and noise $\sigma = 0.042 \pm 0.03$. The M-A biases in the new SSF release are larger than the $\delta \sim (4 \pm 5) \times 10^{-3}$ differences observed in the previous *Terra* Edition 1A MA-comparisons in December 2000 and June 2001 [*Ignatov et al.* 2005]. The results in Figure 15 suggest that for the *Aqua* data, the cross-product correlation is slightly greater than for *Terra* and the noise is smaller, but the bias is somewhat larger.

Ignatov et al. [2005] used the MA-intersection to highlight the M-A *aerosol algorithm* differences. The sampling differences are minimized here compared to the full M and A samples. Note however that they are not removed completely. For instance, Table 3 shows that the average cloud amount in the MA-intersection is still higher in the M product than in the A product: A_T = 46.4% versus 41.1% for *Terra*, and 44.9% versus 39.5% for *Aqua*. This is due to the fact that different CERES footprints are sampled by the M and A products, even within the same 1°-box, and the M product uses different a different cloud mask in selecting pixels.

7.3 Statistical representativeness of the intersection sub-samples

In matching the two data sets as closely as possible in space and time, the intersection sub-sample should remain representative of both full datasets that are being compared. If the condition of statistical representativeness is not met, then the results of comparison ("validation statistics") cannot be extended to represent the full products.

For example, comparison of Table 2 with the respective 1°-rows in Table 1 shows that the size of the *Terra/Aqua* M intersection sub-sample is only 60% of the full *Terra* or *Aqua* M sample, whereas the size of the *Terra/Aqua* A intersection is only ~37% of the full *Terra* or *Aqua* A sample, respectively. The respective statistics of retrievals and auxiliary parameters also differ: in the intersection sample, for instance, A_T is smaller by ~3-4% than in the full M and A samples. A somewhat lower cloud amount is intuitively expected in the *Terra/Aqua* intersection sub-sample, because the requirement that a 1°-box contains at least one cloud-free MODIS pixel from <u>both</u> platforms is more restrictive than the requirement that it is available from <u>at least one</u> platform. Angular domains also differ slightly yet systematically between the full samples and match-up datasets. As a result, τ_{1M} is smaller in the intersection sub-sample by ~0.005, and τ_{1A} by ~0.011 compared to the full samples. Based on these estimates, the *Terra/Aqua* differences obtained from the intersection sub-samples and shown in Figure 14, are probably going to be larger if the full product is considered. The extension of the *Terra/Aqua* match-up statistics to the full sample is less justifiable in the A product where the full and sub-sampled statistics differ more

significantly than in the M product.

The differences between the full sample and its match-up subset are also seen by comparing the statistics of MA intersections in Table 3 with the full samples in Table 1. Typically, the MA intersection is ~96-97% of the full A product but only ~48-52% of the full M product, primarily because of the different VZA restrictions. The statistics of retrievals and auxiliary parameters in the MA-intersection are very close for the A product but significantly differ for the M product (average τ_{1M}=0.133 in the full set versus only τ_{1M}=0.123 in the intersection, cloud amounts are 55.3% versus 46.4%, etc). Therefore, extending statistical conclusions obtained in the MA intersection to the full M sample is less justified than to the full A sample.

The requirement of statistical representativeness is important in many remote sensing applications such as e.g. the validation of satellite products against ground-based sun-photometers. It is often overlooked that the comparisons are done in a relatively small match-up dataset in which both satellite and ground-based data are available. Such match-up datasets are typically more constrained geographically than the *global Terra/Aqua* or MA intersection samples considered above, and may be biased when e.g. mostly coastal stations are used in validation. As a result, one may expect larger differences between the global and local match-up validation statistics than between the two global products discussed above, raising questions about its representativeness of the global satellite product. Certain regions and seasons available in the satellite product are never covered by local ground-based measurements (e.g., many areas in the open ocean, especially in the high latitudes). On the other hand, there may be domains of sun-photometer measurements that are never observed from a satellite, due e.g. to their cloud screening differences. Analyses in this section have demonstrated that it is relatively easy to check the statistical equivalency of the intersection sub-sample and full dataset. However, as of the time of this writing, we are not aware of any validation studies in which such checks were attempted for surface-satellite comparisons.

8. Conclusion

This study compared two global aerosol optical depth products derived from *Terra* and *Aqua*,

using two releases of CERES SSF data. The results shed additional light on the current status of aerosol retrievals and highlights outstanding issues.

Both aerosol products have improved in the latest SSF release. The improvement in the *Terra* M product stems from using collection 4 of MOD04 product, and the improvement in the A product is due to fixing the solar constant values that were erroneously used from *TRMM*/VIRS in the former release. Also, the A sampling has changed, but this does not appear to have any effect on the quality of the A product, except that the size of the A sample is now reduced due to the more conservative A cloud screening.

In the latest release, the *Terra-Aqua* M differences are larger than the A differences. The contrast is statistically significant, and would be even larger if the spatio-temporal noise was removed from the data. The fact that the M cross-platform biases tend to increase in areas that are less populated or more cloudy suggest that residual cloud screening differences between MOD04 and MYD04 are the cause rather than diurnal changes in aerosol abundance between *Terra* and *Aqua* overpass time. In the MOD04 collection 3, this artifact was larger.

The cross-platform noise is also larger in the M product, indicating that generally, the M product is noisier than the A product. The reason for that surprising finding is not immediately clear. Better cross-platform consistency in the A product may be due to a more conservative and cross-platform consistent cloud screening as well as a more restricted view zenith angle range. Another factor, which may possibly contribute here, is that the aerosol model estimated in the M product may be be noisy, especially at typical (low) aerosol loading over ocean. Using the non-variable global aerosol model in the A product may be a more robust approach, which eventually results in less noisy aerosol optical depth. More analyses are needed to explain and resolve this empirical result.

The M and A products are highly correlated from both platforms. Generally, the A algorithm tends to retrieve larger aerosol optical depth. However, as much as half of the resulting aerosol algorithm-induced bias is offset by a more conservative cloud screening in the A product. Complex compensation mechanisms between sampling and aerosol algorithms in the M and A products, which are not fully understood at this time, counter-balance each other and lead to relatively small net differences between the

two global products. Present analyses further support the point made elsewhere that for the overall quality of an aerosol product, especially one included in climate data records, sampling is at least as important as the degree of sophistication and complexity of the aerosol algorithm [*Ignatov et al.* 2005].

It is felt that the current priorities in the aerosol remote sensing should be revisited. In particular, the emphasis should be redirected from the ever increasing level of complexity of the aerosol inversion algorithm towards development of more scientifically sound sampling strategies. The log-normal nature of aerosol optical depth must be considered in pursuing the optimal space-time averaging procedures, validation, and statistical analyses. Cloud screening schemes alternate to the current threshold-based techniques should be explored. In particular, aerosol retrievals in imager pixels contaminated with sub-pixel cloud should be explored, similar to the cloud retrievals in such pixels [*Coakley et al.* 2005]. These efforts would eventually lead to in-depth understanding and unification of the sampling procedures, and more continuous treatment of the "cloud-aerosol" grey zone.

Satellite aerosol *products* are complex combinations of input data, sampling, and aerosol algorithms. These three factors are not fully independent and may interfere in a complicated way. A comprehensive system of quality control/assurance of each *global product* is thus needed that includes a set of self- and cross-consistency checks that are *global* in their nature. Examples of such checks are presented in this paper. These checks are not intended to replace the customary validation against ground-based sun-photometers which is considered the ultimate test for satellite retrievals. Rather, the two techniques should be used in concert with each other. In comparing different datasets using their intersection sub-samples (cross-platform or cross-product comparisons, or validation against ground-truth data), one must ensure that the intersection sample is statistically representative of the full data set being compared or validated.

Acknowledgements. This work was funded by the NASA Science Mission under the CERES Project including NASA contract L-90987C. The *Terra* and *Aqua* CERES SSF data used in this study were obtained from the Atmospheric Sciences Data Center at NASA Langley Research Center. We thank N.

Loeb for his critical support of the proposal to keep two aerosol products on the *Terra* and *Aqua* CERES SSF datasets and helpful discussions, D. Tanré, Y. Kaufman and I. Laszlo for advice, and E. Geier and K. Morris for the help with data access. The views, opinions, and findings contained in this report are those of the authors and should not be construed as an official NOAA or U.S. Government position, policy, or decision.

References

Ackerman S., et al, 1998: Discriminating clears-sky from clouds with MODIS. *JGR*, **103**, 32139-32140.

Brennan, J., Y.Kaufman, I.Koren, and R.Li, 2005: Aerosol-Cloud Interaction – Misclassification of MODIS clouds in heavy aerosol. *IEEE TGARS*, **43**, *4*, doi. 10.1109/TGRS.2005.844662.

Coakley, J., M. Friedman, and W. Tahnk, 2005: Retrieval of cloud properties for partly cloudy imager pixels, *J. Atm. Ocean. Tech.*, 3-17.

Geier E., et al., 2003: CERES data management system: Single Satellite Footprint TOA/Surface fluxes and clouds (SSF) collection document. Release 2, version 1, 212 pp and appendixes. http://asd-www.larc.nasa.gov/ceres/collect_guide/SSF_CG.pdf.

Ichoku, C., L.Remer, and T.Eck, 2005: Quantitative evaluation and intercomparison of morning and afternoon Moderate Resolution Imaging Spectroradiometer (MODIS) aerosol measurements from Terra and Aqua. *JGR*, **110**, *D10*, Art. No. D10S03.

Ignatov, A., 2002: Sensitivity and information content of aerosol retrievals from AVHRR: Radiometric factors. *Appl. Opt.,* **41**, 991-1011.

Ignatov A., I.Laszlo, E.Harrod, K.Kidwell, G.Goodrum, 2004a: Equator crossing times for NOAA, ERS, and EOS sun-synchronous satellites. *Int. J. Remote Sensing*, **25**, *23*, 5255-5266.

Ignatov A., N.Loeb, et al, 2005a: Aerosol retrievals from TRMM/ VIRS over open oceans. *JAM*, in prep.

Ignatov A., P.Minnis, N.Loeb, B.Wielicki, W.Miller, S.Sun-Mack, D.Tanré, L.Remer, I.Laszlo, and E.Geier, 2005: Two MODIS aerosol products over ocean on the Terra and Aqua CERES SSF datasets. *JAS*, 62, 1008-1031.

Ignatov A., J.Sapper, I.Laszlo, N.Nalli, and K.Kidwell, 2004b: Operational Aerosol Observations (AEROBS) from AVHRR/3 onboard NOAA-KLM satellites. *JTech.*, **21**, 3-26.

Ignatov, A., and L. Stowe, 2002a: Aerosol retrievals from individual AVHRR channels. I. Retrievals algorithm and transition from Dave to 6S radiative transfer model. *J. Atm. Sci*, **59**, 313-334.

Ignatov, A., and L. Stowe, 2002b: Aerosol retrievals from individual AVHRR channels. II. Quality control, probability distribution functions and consistency checks of retrievals. *J. Atm. Sci*, **59**, 335-362.

Ignatov, A., L.Stowe, S.Sakerin, and G.Korotaev, 1995: Validation of the NOAA/NESDIS satellite aerosol product over the North Atlantic in 1989. *J. Geophys. Res.*, **100**, 5123-5132.

Kaufman, Y., et al., 2000: Will aerosol measurements form Terra and Aqua polar orbiting satellites represent the daily aerosol abundance and properties? *Geophys. Res. Lett.,* **27**, 3861-3864.

Martins J., et al, 2002: MODIS cloud screening for remote sensing of aerosols over oceans using spatial variability. *GRL,* **29**, 10.1029/2001GL013252.

Matthias, V., and J. Bösenberg, 2002: Aerosol climatology for the planetary boundary layer derived from regular lidar measurements. *Atm. Res.*, **63**, 221-245.

Minnis, P., D. F. Young, S. Sun-Mack, Q. Z. Trepte, R. R. Brown, S. Gibson, and P. Heck, 2004, Diurnal, seasonal, and interannual variations of cloud properties derived for CERES from imager data, *Proc. 13th AMS Conf. Satellite Oceanogr. and Meteorol*., Norfolk, VA, Sept. 20-24, CD-ROM, P6.10.

O'Neill, N., A.Ignatov, B.Holben, and T.Eck, 2000: The log-normal distribution as a reference for reporting aerosol optical depth statistics: Empirical tests using multi-year, multi-site AERONET sun photometer data. *Geophys. Res. Lett.*, **27**, 4778, 3333-3336.

Remer, L., et al., 2002: Validation of MODIS aerosol retrievals over ocean. *Geophys. Res. Lett.*, **29**, 8008, doi:10.1029/2001GL013204.

Remer, L., Y.Kaufman, S.Mattoo, V.Martins, C.Ichoku, R.Levy. and R.Kleidman, 2005: The MODIS Aerosol Algorithm, Products, and Validation. *JAS*, **62**, *4*, 947-973

Szewcyzk, Z. P., G. L. Smith, and K. J. Priestley, 2005: Validation of Clouds and Earth Radiant Energy System instruments aboard the *Terra* and *Aqua* satellites, *J. Geophys. Res.*, *110,* D02103, doi:10.1029/2004JD004776.

Tanré D., et al, 1997: Remote sensing of aerosol properties over oceans using the MODIS/EOS spectral radiances. *JGR*, **102**, 16,971-16,988.

Wielicki B., et al, 1996: Clouds and the Earth's Radiant Energy System (CERES): An Earth Observing System Experiment. *BAMS*, **77**, *11*, 853-868.

Table captions

Table 1. Global mean counts and statistics of τ_{1M}, τ_{1A} and auxiliary parameters [LT-local time; LAT-latitude; LON-longitude; A_T-cloud amount, determined by the A-processing; θ_V-nadir view angle, calculated with its sign indicating side of the orbit ("+": anti-solar, "-": solar); θ_S-solar zenith angle; χ–scattering angle; γ–glint angle] in CERES SSF *Terra* Edition 2A and *Aqua* Edition 1B data from 13-21 October 2002 based on CERES FOVs (odd rows) and 1°-boxes (even rows).

Table 2. Global mean statistics of τ_{1M}, τ_{1A} and auxiliary parameters in the M and A *Terra/Aqua* intersection data sets from 13-21 October 2002.

Table 3. Global mean statistics of τ_{1M}, τ_{1A} and auxiliary parameters in the MA intersection data sets for *Terra* and *Aqua* from 13-21 October 2002.

Table 1. Global mean counts and statistics of τ_{1M}, τ_{1A} and auxiliary parameters [LT-local time; LAT-latitude; LON-longitude; A_T-cloud amount, determined by the A-processing; θ_V-nadir view angle, calculated with its sign indicating side of the orbit ("+": anti-solar, "-": solar); θ_S-solar zenith angle; χ–scattering angle; γ–glint angle] in CERES SSF *Terra* Edition 2A and *Aqua* Edition 1B data from 13-21 October 2002 based on CERES FOVs (odd rows) and $(1°)^2$-boxes (even rows).

Terra/M	N	τ_{1M}	LT, h	A_T, %	θ_V, °	θ_S, °	χ, °	γ, °
CERES FOVs	2,008,739	0.129	10.41	48.2	10.6	37.9	135.6	62.6
$(1°)^2$-boxes	164,895	0.138	10.41	55.3	7.1	38.3	131.7	64.3
Aqua/M	N	τ_{1M}	LT, h	A_T, %	θ_V, °	θ_S, °	χ, °	γ, °
CERES FOVs	1,806,763	0.120	13.73	46.4	15.2	43.1	139.2	66.3
$(1°)^2$-boxes	145,395	0.125	13.73	54.0	12.0	43.9	134.3	68.3
Terra/A	N	τ_{1A}	LT, h	A_T, %	θ_V, °	θ_S, °	χ, °	γ, °
CERES FOVs	932,810	0.133	10.17	32.5	32.6	37.3	149.8	64.2
$(1°)^2$-boxes	81,426	0.135	10.08	41.3	36.7	39.5	146.7	69.2
Aqua/A	N	τ_{1A}	LT, h	A_T, %	θ_V, °	θ_S, °	χ, °	γ, °
CERES FOVs	951,832	0.130	13.90	30.6	30.2	42.0	152.5	68.2
$(1°)^2$-boxes	80,573	0.132	13.99	39.9	34.7	44.1	150.1	74.0

Table 2. Global mean statistics of τ_{1M}, τ_{1A} and auxiliary parameters in the M and A *Terra/Aqua* intersection data sets from 13-21 October 2002.

Terra/Aqua M	N	τ_{1M}	LT, h	A_T, %	θ_V, °	θ_S, °	χ, °	γ, °
Terra	96,275	0.132	10.45	53.3	5.4	39.9	130.2	63.6
Aqua	96,275	0.121	13.64	51.9	9.2	44.8	132.2	67.1
Terra/Aqua A	N	τ_{1A}	LT, h	A_T, %	θ_V, °	θ_S, °	χ, °	γ, °
Terra	29,742	0.124	10.07	38.1	36.6	40.4	145.6	69.3
Aqua	29,742	0.120	13.97	35.7	34.2	45.3	148.2	74.1

Table 3. Global mean statistics of τ_{1M}, τ_{1A} and auxiliary parameters in the MA intersection data sets for *Terra* and *Aqua* from 13-21 October 2002.

MA Terra	N	τ_{1M}/τ_{1A}	LT, h	A_T, %	θ_V, °	θ_S, °	χ, °	γ, °
M	79,209	0.123	10.17	46.4	30.5	39.0	144.7	67.6
A	79,209	0.134	10.07	41.1	36.9	39.4	146.8	69.3
MA Aqua	N	τ_{1M}/τ_{1A}	LT, h	A_T, %	θ_V, °	θ_S, °	χ, °	γ, °
M	77,262	0.118	13.92	44.9	29.8	43.7	147.9	72.1
A	77,262	0.131	14.00	39.4	34.8	44.1	150.2	74.2

Figure captions

Figure 1. Local equator crossing time, η(h), for the *Terra* and *Aqua* platforms. Data are the two-line element from www.celestrak.com. Note that the nominal EXTs are 1030 for *Terra* and 0130 for *Aqua*. For details, see (Ignatov et al. 2004a).

Figure 2. Frequency of local solar time in the M and A aerosol observations from *Terra* and *Aqua* platforms. Note that the solar side of orbit is excluded from the A product. As a result, its histogram is mono-modal and shifted with respect to the equator crossing time towards lower Sun. The second peak in the M product comes from the solar side of the orbit.

Figure 3. Top: count of CERES FOVs in 1°-boxes in the (left) M and (right) A products. Bottom: trends in the mean and minimum AOD: (left) τ_{1M} and (right) τ_{1A} from *Terra* (squares/broken lines) and *Aqua* (circles/solid lines). Note that τ_{1M} are truncated in the M*D04 processing and therefore min(τ_{1M}) never goes below zero. The τ_{1A} are not truncated and may go negative. (Physical origin of negative τ_A is discussed in Ignatov and Stowe 2002.) Trends in τ_{1A} are smaller and more cross-platform consistent compared to τ_{1M}. Divergence between *Terra/Aqua* τ_{1M}-trends at N<20 may be due to residual cloud screening differences between MOD04 and MYD04. Close agreement between min(τ_{1A}) in MODIS band1 from *Terra* and *Aqua* 1indicates excellent cross-platform calibration consistency (Ignatov 2002).

Figure 4. Global distribution of τ_{1M} and τ_{1A} derived from 1° *Terra* and *Aqua* data and averaged over the 9-day period from 13-21 October 2002.

Figure 5. Top: Zonal density of M and A retrievals (bin size $\Delta\varphi$=5°). Note that spatial coverage from *Terra* and *Aqua* is similar in both M and A products. Bottom: trends in the respective τ_{1M} and τ_{1A}. Note

that the A product shows more cross-platform consistency than the M product.

Figure 6. Top: Histograms of τ_{1M} and τ_{1A} derived from the *current release* CERES SSF 1° *Terra* (Edition 2A) and *Aqua* (Edition 1B) global data from 13-21 October 2002. Geometric mean and STD statistics are superimposed. Bottom: Same but for $\log(\tau_{1M})$and $\log(\tau_{1A})$. In addition to geometric mean and STD statistics, skewness (*s*) and kurtosis (*k*) are also shown. (Note that for a Gaussian distribution, *s=k=0.*)

Figure 7. Same as in Figure 6 but using data from the previous SSF release, which employed the same aerosol algorithms but different M and A preprocessing and sampling. In particular, the *Terra* M product was based on MOD04 collection 3 (the latest release shown in Figure 6 is based on collection 4.) The SSF processing is based on 1-km data sub-sampled in every 2nd column and every 2nd row (the current release shown in Figure 6 sub-samples every 4th pixel in every 2nd row.) Also a ~4% solar flux error in the A product was fixed in the latest SSF release. See section 4 for further discussion.

Figure 8. Same as in Figure 3 but for the ambient cloud amount, A_T (binned at ΔA_T=5%). Note that A_T was determined by the A-cloud screening. For the exact definition of A_T and for relevant discussion see section 4.1. In the M product, maximum of the A_T-histograms is found in the highest bin centered at A_T~97.5% (includes data with $95 \le A_T < 100\%$), whereas in the A-product, it is in the lowest bin at A_T~2.5% (includes data with $0 \le A_T < 5\%$). The average A_T is ~47% in the M products compared to A_T~32% in the A-product (cf. data in Table 1). The τ_{1A}-trends are smaller compared with τ_{1M} trends, and more reproducible cross-platform. Small divergence between the two τ_{1M} trends towards larger A_T's may indicate residual cloud screening differences in the M product between the two platforms (cf. τ_{1M}(N) trends in Figure 3).

Figure 9. Same as in Figure 8 but using data from the previous SSF release (see caption to Figure 7 for

more detail on the release difference). Note the following differences with the previous release: (a) Cross-platform differences in the M product are larger than in Figure 8 (cf. histograms and $\tau_{1M}(A_T)$ trends at large A_T); (b) The A-histograms extend further into large A_T domain, and are less cross platform consistent than in Figure 8; τ_{1A} at A_T~0% is ~0.02 smaller than in Figure 8.

Figure 10. Top: Histograms of view angle in (left) M and (right) A products (bin size $\Delta\theta_V$=8°). Note that view angle is defined as negative on the solar side of orbit and positive on the anti-solar side. View angle domains from *Terra* and *Aqua* are similar, but differ between M and A products. Bottom: View angle trends in τ_{1M} and τ_{1A}. Note that the A product is more cross-platform consistent than the M product, which develops cross-platform differences on the solar side of orbit.

Figure 11. Same as in Figure 10 but for the solar zenith angle (bin size $\Delta\theta_S$=5°). Retrievals from *Aqua* are made at a lower Sun than from *Terra*. Range of Sun angle is wider in M than in A products. Trends in τ_{1M} are cross-platform consistent but the curves are systematically shifted by ~0.01. The τ_{1A} trends are consistent except at very high Sun (<35°). Low bias in τ_{1M} and τ_{1A} at Sun angle (>50°) maybe due to correlation with geography (high latitude clean open ocean areas), or increased cloud screening difficulties and violation of plane parallel radiative transfer assumption used in 6S.

Figure 12. Same as in Figure 10 but for the scattering angle (bin size $\Delta\chi$=5°). Retrieval domains from *Aqua* and *Terra* are close, with *Aqua* being slightly shifted towards backscatter. Range of scattering angle is wider in the M than in the A product. Trends in τ_{1M} are cross-platform consistent in both products, and larger in the A product. Part of trends may be due to correlation with geography

Figure 13. Same as in Figure 10 but for the glint angle (bin size $\Delta\gamma$=5°). Note that in both products, retrievals are not made at γ<40°. Retrieval domains from *Aqua* and *Terra* are close with *Aqua* being

further away from the glint area. Range of glint angle is wider in the M than in the A product. Both product diverge at γ>90-100° and the M product additionally diverge at 40°<γ<65°.

Figure 14. Cross-platform analyses of τ_{1M} and τ_{1A} derived from 1° *Terra-Aqua* match-up datasets (see statistics in Table 2): (a1) scattergram of *Terra* τ_{1M} versus *Aqua* τ_{1M} (correlation coefficient, R, superimposed); (b1) same as (a1) but for τ_{1A}; (a2-b2) same as (a1-b1) but for $\lg\tau_1$; (a3) histogram of *Terra-Aqua* τ_{1M} difference (mean, δ, and STD, σ, statistics are superimposed); (b3) same as (a3) but for τ_{1A}; (a4-b4) same as (a3-b3) but for $\lg\tau_1$. Note that τ_{1A} shows higher cross-platform correlation, and smaller bias and RMSD.

Figure 15. Cross-product analyses of τ_{1M} and τ_{1A} derived from 1° *Terra-Aqua* match-up datasets (see statistics in Table 3): (a1) scattergram of τ_{1A} versus τ_{1M} for *Terra* (correlation coefficient, R, superimposed); (b1) same as (a1) but for *Aqua*; (a2-b2) same as (a1-b1) but for $\lg\tau_1$; (a3) histogram of -τ_{1A}-τ_{1M} difference for *Terra* (mean, δ, and STD, σ, statistics are superimposed); (b3) same as (a3) but for *Aqua*; (a4-b4) same as (a3-b3) but for $\ln\tau_1$. Note that τ_{1A} shows higher cross-platform correlation, and smaller bias and RMSD.

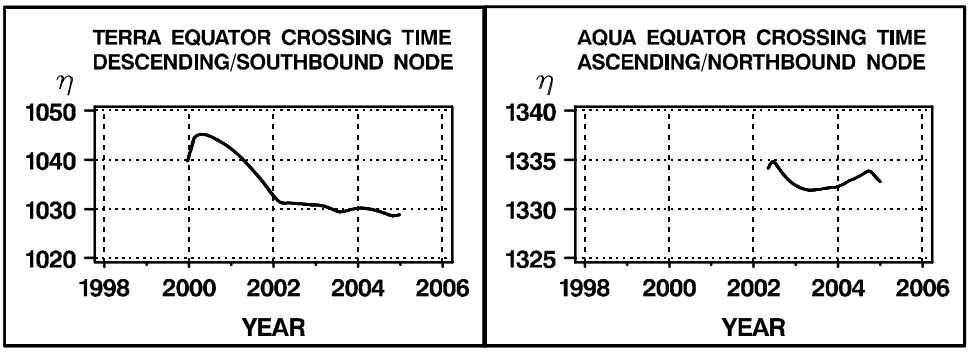

Figure 1. Local equator crossing time, η(h), for the *Terra* and *Aqua* platforms. Data are the two-line element from www.celestrak.com. Note that the nominal EXTs are 1030 for *Terra* and 0130 for *Aqua*. For details, see (Ignatov et al. 2004a).

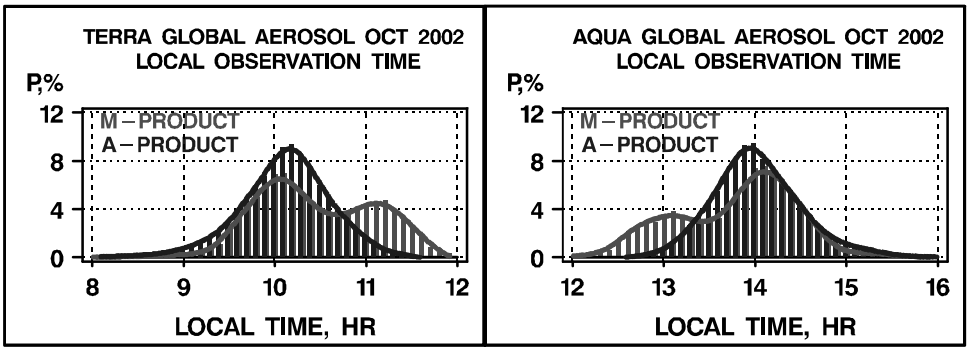

Figure 2. Frequency of local solar time in the M and A aerosol observations from *Terra* and *Aqua* platforms. Note that the solar side of orbit is excluded from the A product. As a result, its histogram is mono-modal and shifted with respect to the equator crossing time towards lower Sun. The second peak in the M product comes from the solar side of the orbit.

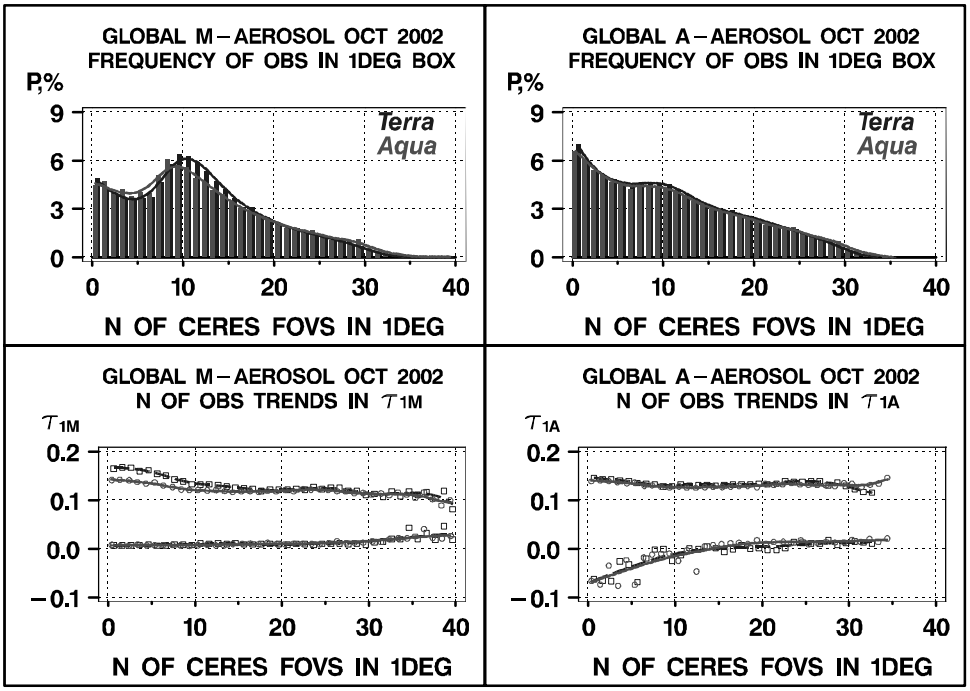

Figure 3. Top: count of CERES FOVs in $(1°)^2$-boxes in the (left) M and (right) A products. Bottom: trends in the mean and minimum AOD: (left) τ_{1M} and (right) τ_{1A} from *Terra* (squares/broken lines) and *Aqua* (circles/solid lines). Note that τ_{1M} are truncated in the M*D04 processing and therefore min(τ_{1M}) never goes below zero. The τ_{1A} are not truncated and may go negative, mainly due to radiometric errors or overestimated Rayleigh contribution over high-altitude lakes (Ignatov and Stowe 2002a). Trends in τ_{1A} are smaller and more cross-platform consistent compared to τ_{1M}. Divergence between *Terra/Aqua* τ_{1M}-trends at N<20 may be due to residual cloud screening differences between MOD04 and MYD04. Close agreement between min(τ_{1A}) in MODIS band 1 from *Terra* and *Aqua* 1indicates excellent cross-platform calibration consistency (Ignatov 2002).

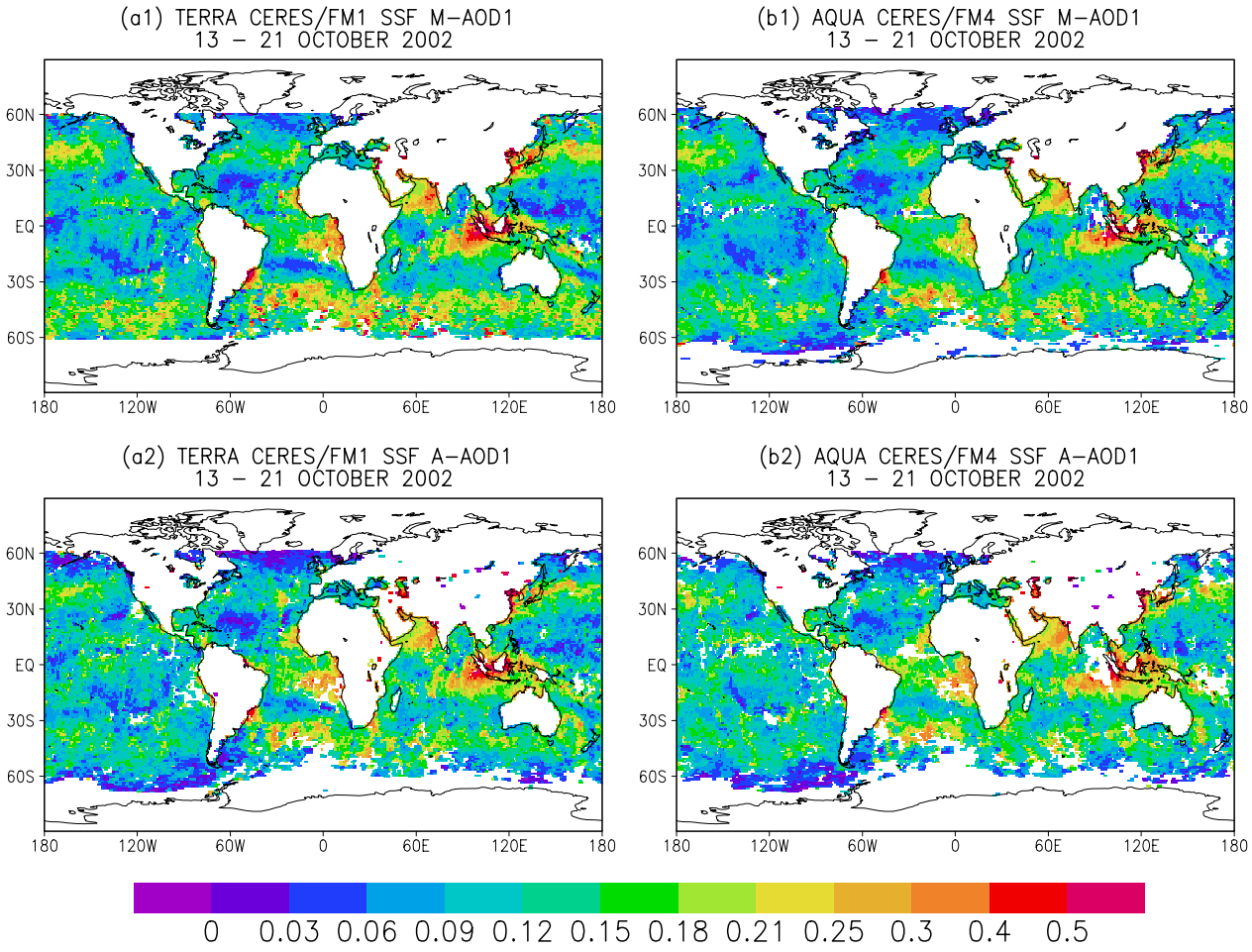

Figure 4. Global distribution of τ_{1M} and τ_{1A} derived from $(1°)^2$ *Terra* and *Aqua* data and averaged over the 9-day period from 13-21 October 2002.

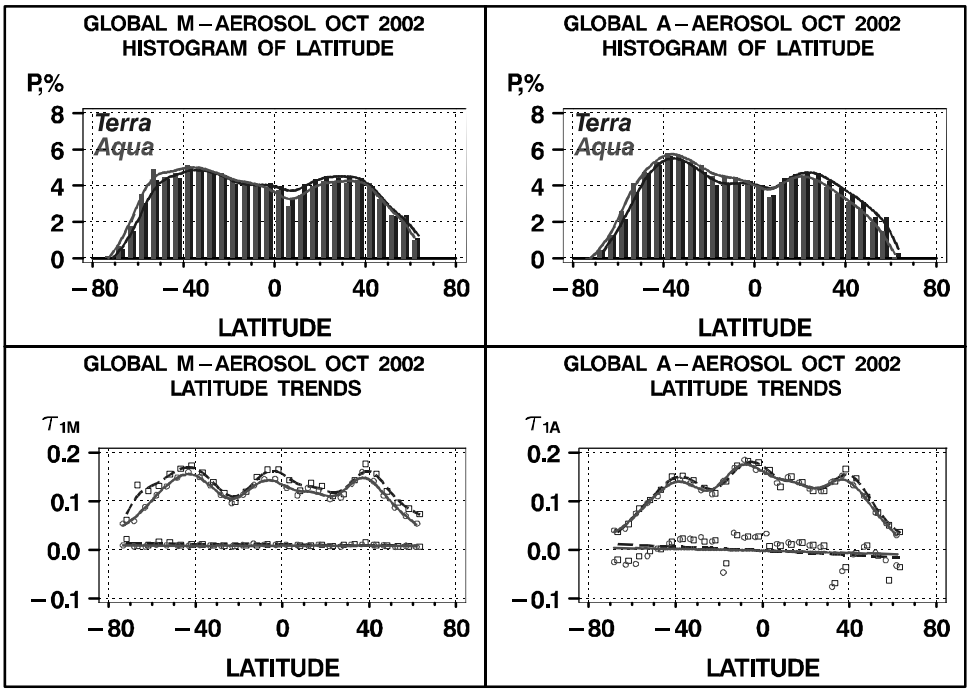

Figure 5. Top: Zonal density of M and A retrievals (bin size $\Delta\varphi=5°$). Note that spatial coverage from *Terra* and *Aqua* is similar in both M and A products. Bottom: trends in the respective τ_{1M} and τ_{1A}. Note that the A product shows more cross-platform consistency than the M product.

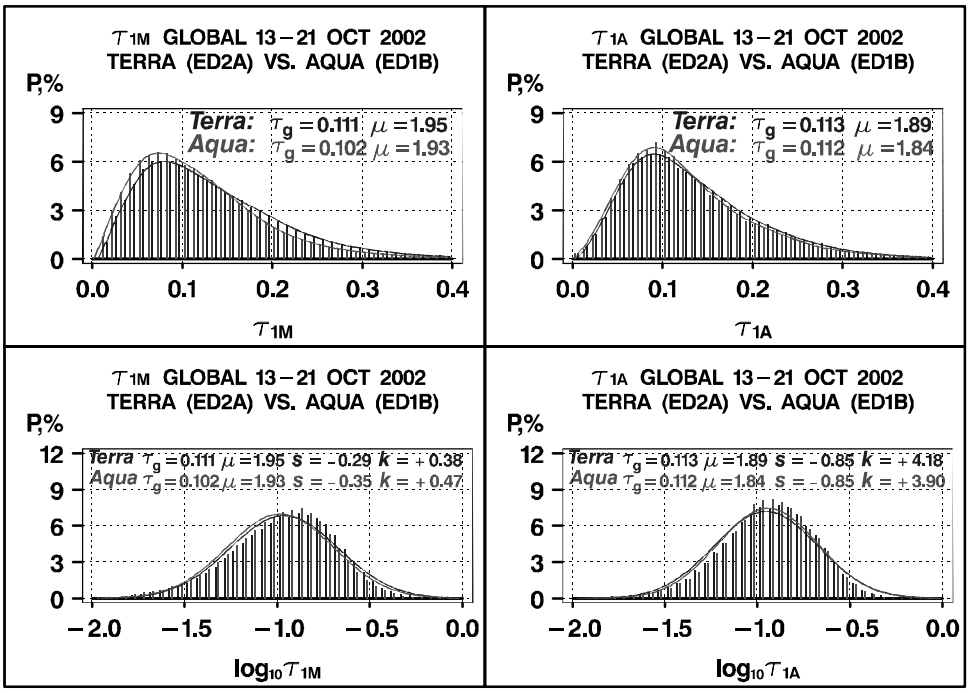

Figure 6. Top: Histograms of τ_{1M} and τ_{1A} derived from the current release CERES SSF $(1°)^2$ *Terra* (Edition 2A) and *Aqua* (Edition 1B) global data from 13-21 October 2002. Geometric mean and STD statistics are superimposed. Bottom: Same but for $\log(\tau_{1M})$and $\log(\tau_{1A})$. In addition to geometric mean and STD statistics, skewness (*s*) and kurtosis (*k*) are also shown. (Note that for a Gaussian distribution, *s=k=0*.)

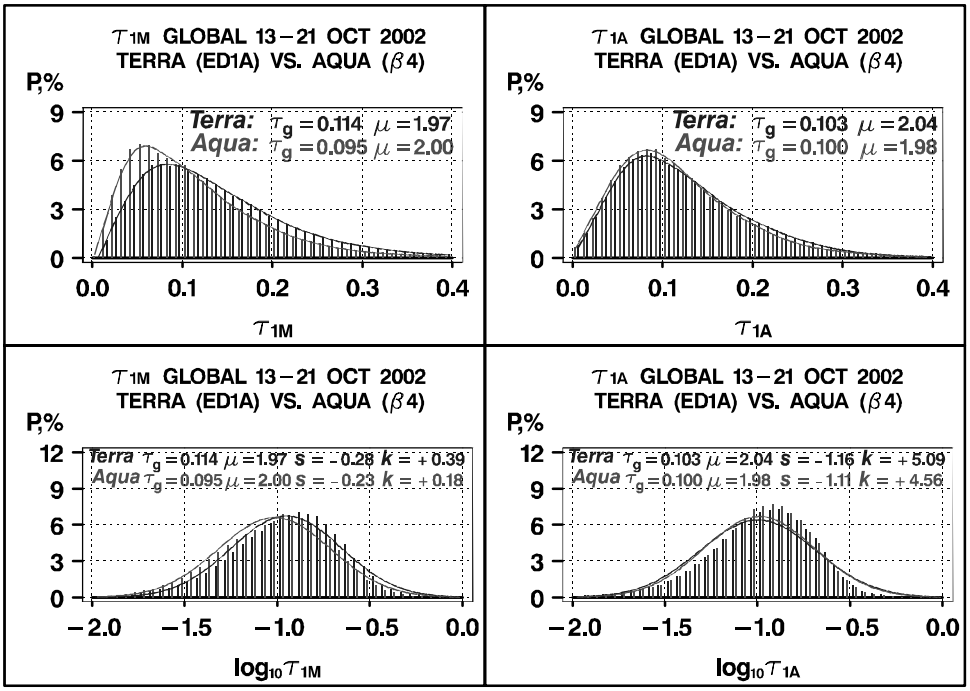

Figure 7. Same as in Fig. 6 but using data from the previous SSF release, which employed the same aerosol algorithms but different M and A preprocessing and sampling. In particular, the *Terra* M product was based on MOD04 collection 3 (the latest release shown in Fig. 6 is based on collection 4.) The SSF processing is based on 1-km data sub-sampled in every 2nd column and every 2nd row (the current release shown in Fig. 6 sub-samples every 4th pixel in every 2nd row.) Also a ~4% solar flux error in the A product was fixed in the latest SSF release. See section 4 for further discussion.

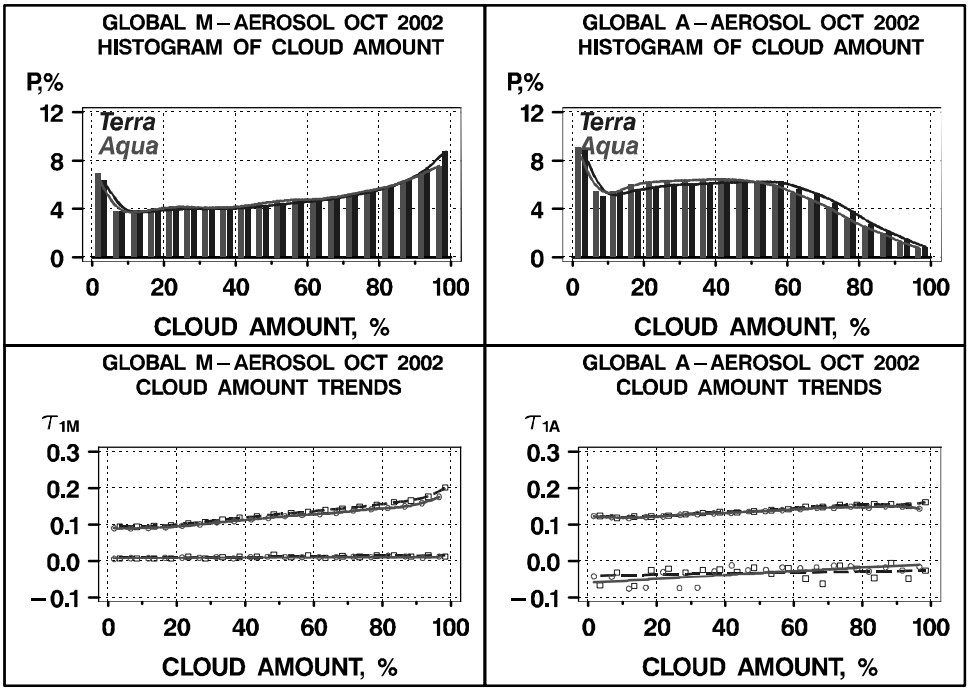

Figure 8. Same as in Fig. 3 but for the ambient cloud amount, A_T (binned at ΔA_T=5%). Note that A_T was determined by the A-cloud screening. For the exact definition of A_T and for relevant discussion see section 4.1. In the M product, maximum of the A_T-histograms is found in the highest bin centered at A_T~97.5% (includes data with $95 \le A_T < 100\%$), whereas in the A-product, it is in the lowest bin at A_T~2.5% (includes data with $0 \le A_T < 5\%$). The average A_T is ~47% in the M products compared to A_T~32% in the A-product (cf. data in Table 1). The τ_{1A}-trends are smaller compared with τ_{1M} trends, and more reproducible cross-platform. Small divergence between the two τ_{1M} trends towards larger A_T's may indicate residual cloud screening differences in the M product between the two platforms (cf. τ_{1M}(N) trends in Fig. 3).

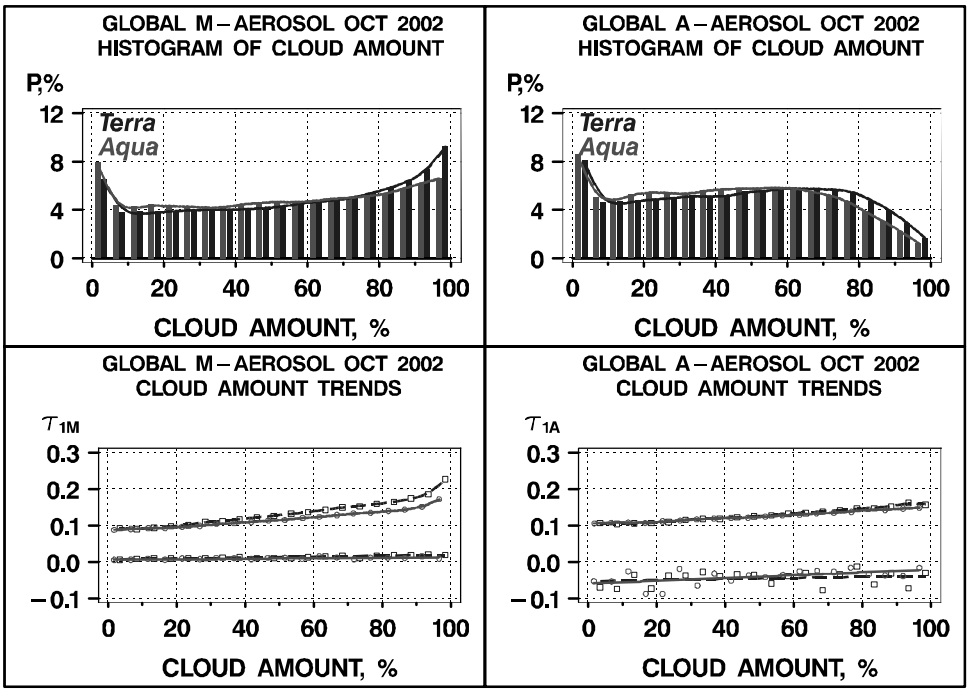

Figure 9. Same as in Fig. 8 but using data from the previous SSF release (see caption to Fig. 7 for more detail on the release difference). Note the following differences with the previous release: (a) Cross-platform differences in the M product are larger than in Fig. 8 (cf. histograms and $\tau_{1M}(A_T)$ trends at large A_T); (b) The A-histograms extend further into large A_T domain, and are less cross platform consistent than in Fig. 8; τ_{1A} at A_T~0% is ~0.02 smaller than in Fig. 8.

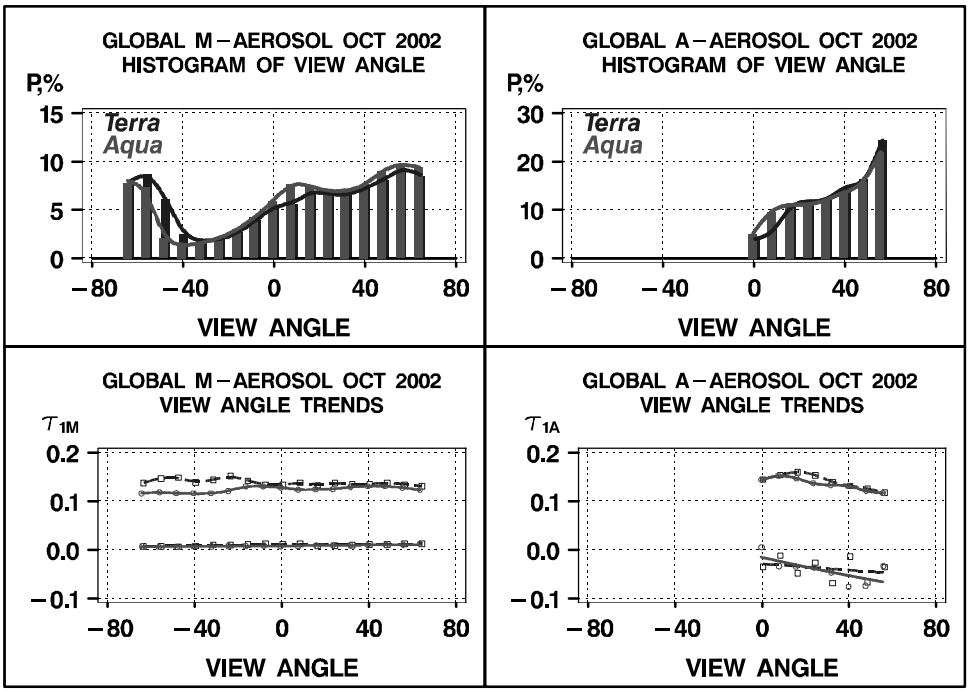

Figure 10. Top: Histograms of view angle in (left) M and (right) A products (bin size $\Delta\theta_V$=8°). Note that view angle is defined as negative on the solar side of orbit and positive on the anti-solar side. View angle domains from *Terra* and *Aqua* are similar, but differ between M and A products. Bottom: View angle trends in τ_{1M} and τ_{1A}. Note that the A product is more cross-platform consistent than the M product, which develops cross-platform differences on the solar side of orbit.

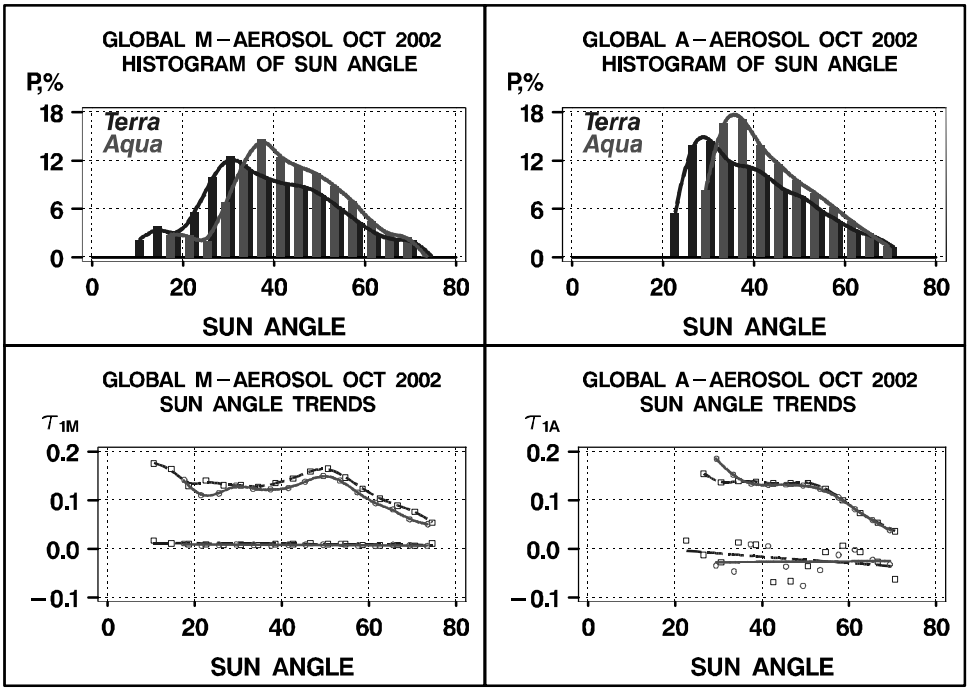

Figure 11. Same as in Fig. 10 but for the solar zenith angle (bin size $\Delta\theta_S$=5°). Retrievals from *Aqua* are made at a lower Sun than from *Terra*. Range of Sun angle is wider in M than in A products. Trends in τ_{1M} are cross-platform consistent but the curves are systematically shifted by ~0.01. The τ_{1A} trends are consistent except at very high Sun (<35°). Low bias in τ_{1M} and τ_{1A} at Sun angle (>50°) maybe due to correlation with geography (high latitude clean open ocean areas), or increased cloud screening difficulties and violation of plane parallel radiative transfer assumption used in 6S.

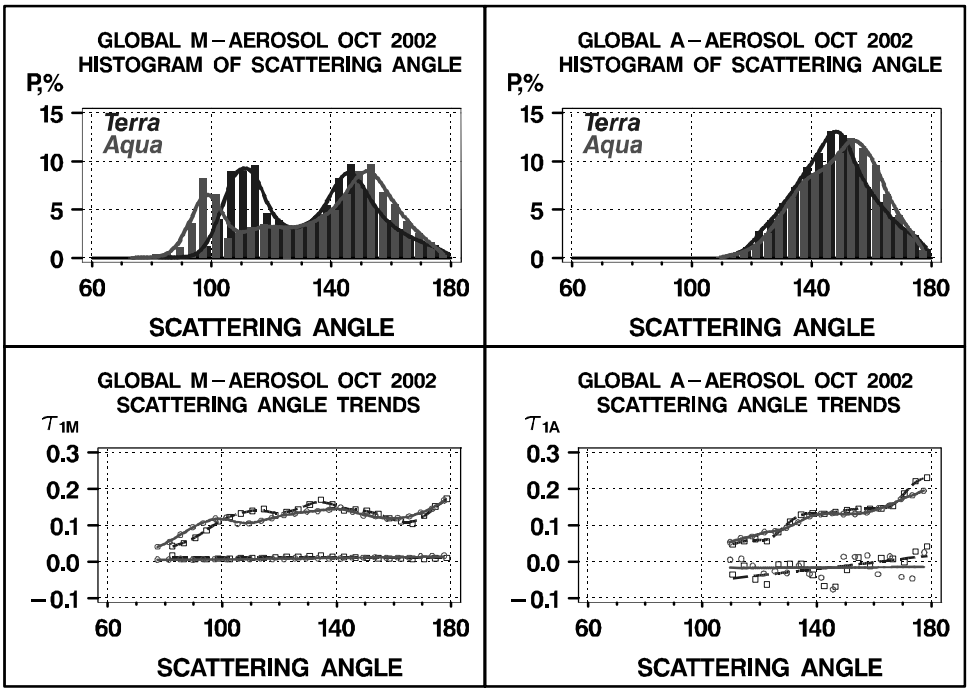

Figure 12. Same as in Fig. 10 but for the scattering angle (bin size $\Delta\chi$=5°). Retrieval domains from *Aqua* and *Terra* are close, with *Aqua* being slightly shifted towards backscatter. Range of scattering angle is wider in the M than in the A product. Trends in τ_{1M} are cross-platform consistent in both products, and larger in the A product. Part of trends may be due to correlation with geography.

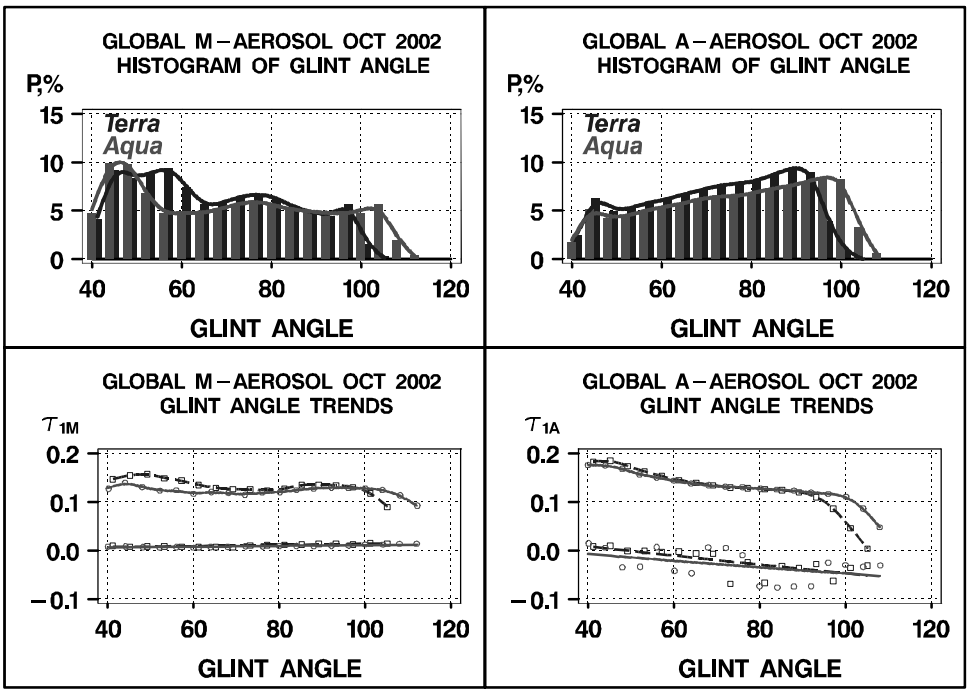

Figure 13. Same as in Fig. 10 but for the glint angle (bin size $\Delta\gamma=5°$). Note that in both products, retrievals are not made at $\gamma<40°$. Retrieval domains from *Aqua* and *Terra* are close with *Aqua* being further away from the glint area. Range of glint angle is wider in the M than in the A product. Both product diverge at $\gamma>90$-$100°$ and the M product additionally diverge at $40°<\gamma<65°$.

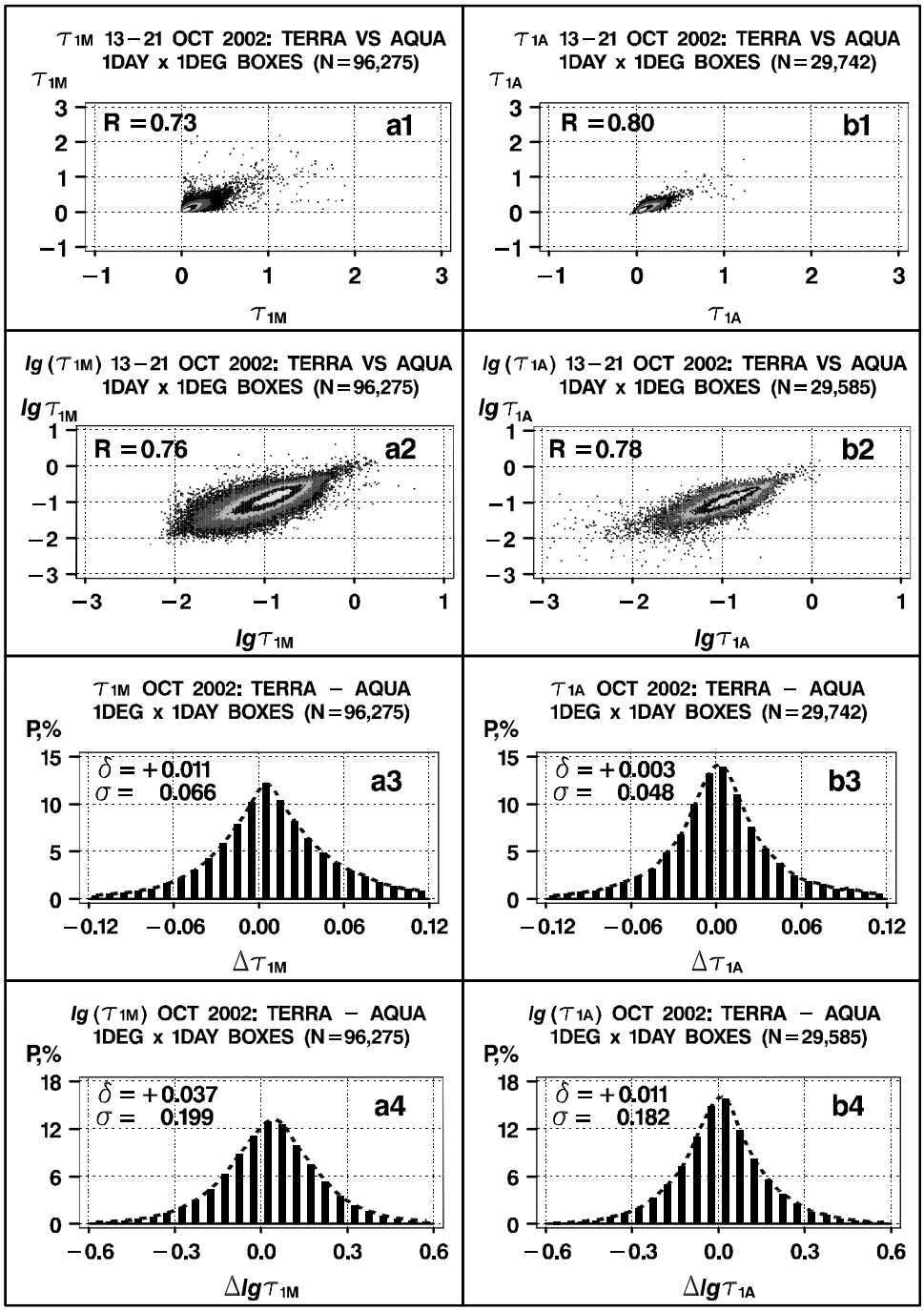

Fig. 14. Cross-platform analyses of τ_{1M} and τ_{1A} derived from $(1°)^2$ *Terra-Aqua* match-up datasets (see statistics in Table 2): (a1) scattergram of *Terra* τ_{1M} versus *Aqua* τ_{1M} (correlation coefficient, R, superimposed); (b1) same as (a1) but for τ_{1A}; (a2-b2) same as (a1-b1) but for $\lg\tau_1$; (a3) histogram of *Terra-Aqua* τ_{1M} difference (mean, δ, and STD, σ, statistics are superimposed); (b3) same as (a3) but for τ_{1A}; (a4-b4) same as (a3-b3) but for $\lg\tau_1$. Note that τ_{1A} shows higher cross-platform correlation, and smaller bias and RMSD.

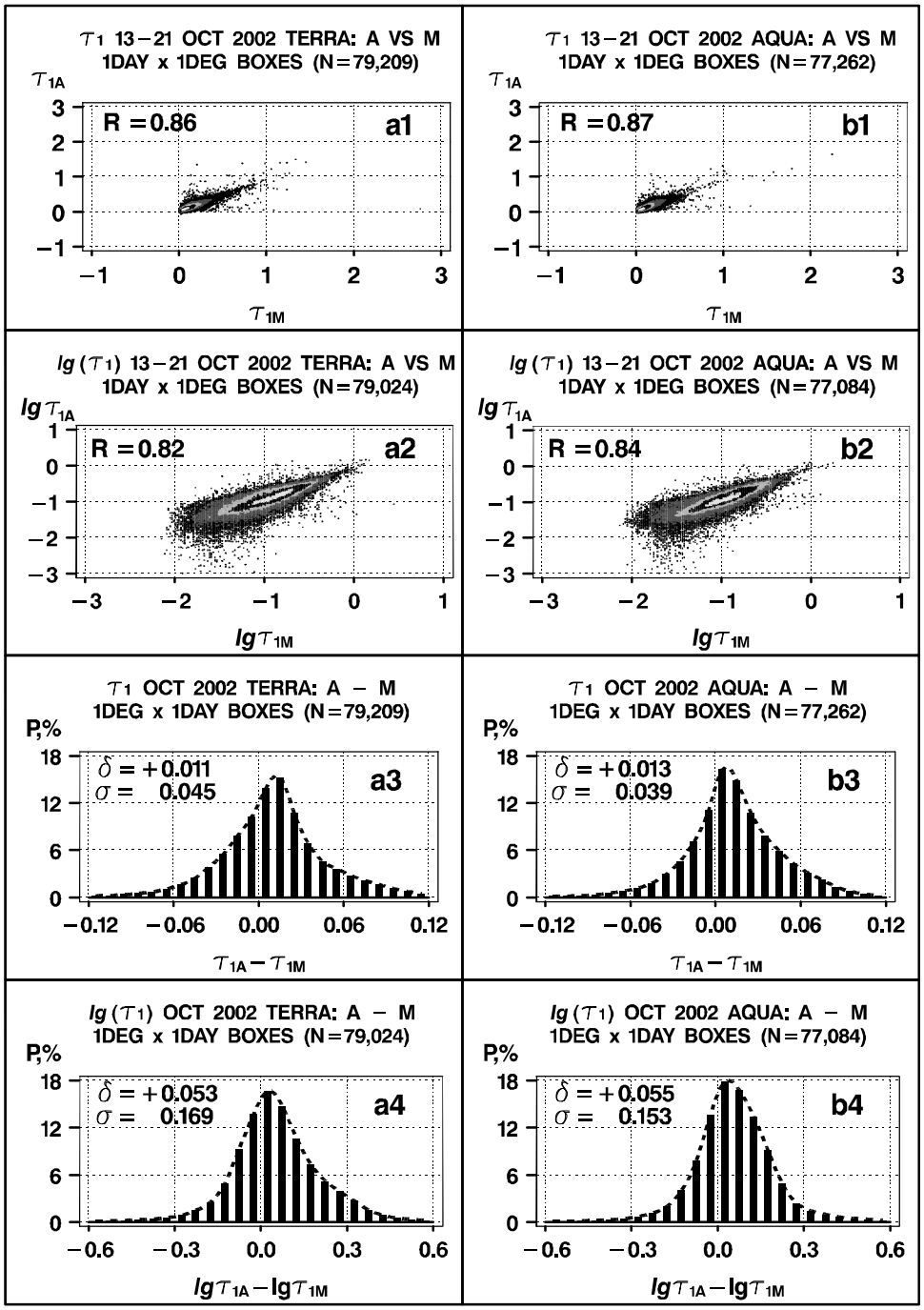

Fig. 15. Cross-product analyses of τ_{1M} and τ_{1A} derived from $(1°)^2$ *Terra-Aqua* match-up datasets (see statistics in Table 3): (a1) scattergram of τ_{1A} versus τ_{1M} for *Terra* (correlation coefficient, R, superimposed); (b1) same as (a1) but for *Aqua*; (a2-b2) same as (a1-b1) but for $\lg\tau_1$; (a3) histogram of - τ_{1A}-τ_{1M} difference for *Terra* (mean, δ, and STD, σ, statistics are superimposed); (b3) same as (a3) but for *Aqua*; (a4-b4) same as (a3-b3) but for $\lg\tau_1$. Note that τ_{1A} shows higher cross-platform correlation, and smaller bias and RMSD.